Chapter 7

Impacts of the Tibetan Plateau on Asian Climate

GUOXIONG WU AND YIMIN LIU

State Key Laboratory of Numerical Modeling for Atmospheric Sciences and Geophysical Fluid Dynamics (LASG), Institute of Atmospheric Physics, Chinese Academy of Sciences, Beijing, China

ABSTRACT

Professor Yanai is remembered in our hearts as an esteemed friend. Based on his accomplishments in tropical meteorology and with his flashes of insight he led his group at the University of California, Los Angeles, in the 1980s and 1990s to explore the thermal features of the Tibetan Plateau (TP) and its relation to the Asian monsoon, and he brought forward the TP meteorology established by Ye Duzheng et al. in 1957 to a new stage. In cherishing the memory of Professor Yanai and his great contribution to the TP meteorology, the authors review their recent study on the impacts of the TP and contribute this chapter as an extension of their chapter titled ''Effects of the Tibetan Plateau'' published by Yanai and Wu in 2006 in the book *The Asian Monsoon*.

The influence of a large-scale orography on climate depends not only on the mechanical and thermal forcing it exerts on the atmosphere, but also on the background atmospheric circulation. In winter the TP possesses two leading heating modes resulting from the relevant dominant atmospheric circulations, in particular the North Atlantic Oscillation and the North Pacific Oscillation. The prevailing effect of the mechanical forcing of the TP in wintertime generates a dipole type of circulation, in which the anticyclonic gyre in the middle and high latitudes contributes to the warm inland area to the west, and the cold seashore area to the east, of northeast Asia, whereas the cyclonic gyre in low latitudes contributes to the formation of a prolonged dry season over central and southern Asia and moist climate over southeastern Asia. Such a dipole circulation also generates a unique persistent rainfall in early spring (PRES) over southern China.

In 1980s, Yanai and his colleagues analyzed the in situ observation and found that the constant potential temperature boundary layer over the TP can reach about 300 hPa before the summer monsoon onset. This study supports these findings, and demonstrates that such a boundary layer structure is a consequence of the atmospheric thermal adaptation to the surface sensible heating, which vanishes quickly with increasing height. The overshooting of rising air, which is induced by surface sensible heating, then can form a layer of constant potential temperature with a thickness of several kilometers.

The thermal forcing of the TP on the lower tropospheric circulation looks like a sensible heat–driven air pump (SHAP). It is the surface sensible heating on the sloping sides of the plateau that the SHAP can effectively influence the Asian monsoon circulation. In spring the SHAP contributes to the seasonal abrupt change of the Asian circulation and anchors the earliest Asian summer monsoon onset over the eastern Bay of Bengal. In summer, this pumping, together with the thermal forcing over the Iranian Plateau, produces bimodality in the South Asian high activity in the upper troposphere, which is closely related to the climate anomaly patterns over South and East Asia. Because the isentropic surfaces in the middle and lower troposphere intersect with the TP, in summertime the plateau becomes a strong negative vorticity source of the atmosphere and affects the surrounding climate and even the Northern Hemispheric circulation via Rossby wave energy dispersion. Future prospects in related TP studies are also addressed.

Corresponding author address: Guoxiong Wu, Institute of Atmospheric Physics, LASG, 40 HuayanBeili, Chaoyang District, Beijing, 9804, China.
E-mail: gxwu@lasg.iap.ac.cn

DOI: 10.1175/AMSMONOGRAPHS-D-15-0018.1

1. Introduction

Monsoons are generally considered an atmospheric response to seasonal changes in land–sea thermal contrast induced by the annual cycle of the solar zenith angle (Wallace and Hobbs 1977; Holton 2004). The Asian summer monsoon (ASM) is the strongest element of the global monsoon system (Flohn 1957; Chang 2004; Wang 2006). In addition to land–sea thermal contrast, it is affected by large-scale mountain ranges such as the Tibetan Plateau (TP) (Yeh et al. 1957; Ye and Gao 1979; Yanai et al. 1992; Yanai and Wu 2006). The TP, also called the Qinghai-Xizang Plateau in China, extends over the area of 27°–45°N, 70°–105°E, covering a region about one-quarter the size of the entire Chinese territory. Its mean elevation is more than 4000 m above sea level, with the peak of Mount Everest at 8844 m (near 300 hPa) standing on its southern fringe. In winter the TP together with the Iranian Plateau serves as a giant wall across almost the whole Eurasian continent that blocks cold outbreaks from the north and confines the winter monsoon to eastern and southern Asia (Chang et al. 2006).

Yanai and Wu (2006) gave a thorough review of the past studies about the effects of the TP. The review starts from the research in the 1950s on the jet stream and the warm South Asian high, and the early progress of TP research. The review then goes over studies concerning the mechanical effects of the TP on large-scale motion, the winter cold surge, and the summer negative vorticity source over the TP. The review also covers the importance of the thermal influences of the TP on the seasonal circulation transition and Asian monsoon onset based on different datasets and numerical experiments (Ye and Gao 1979; Tao and Chen 1987; Wu et al. 1997, 2002; X. Liu et al. 2001; Y. Liu et al. 2001; Liu et al. 2002; Mao et al. 2002a,b; Wang and LinHo 2002). This paper is an effort to review the evaluation of the heating source on the TP through the analyses of spatial and temporal distributions of $\langle Q_1 \rangle$ and $\langle Q_2 \rangle$ in the notation used by Yanai et al. (1973) and based on observations from the First GARP Global Experiment (FGGE) (December 1978–November 1979) and the Qinghai–Xizang Plateau Meteorology Experiment (QXPMEX), conducted from May to August 1979 by Chinese meteorologists (Zhang et al. 1988).

Since then, great efforts have been made to understand the mechanism concerning how the TP forcing, either mechanical or thermodynamical, can affect the regional as well as global climate. Some of the results are summarized in this study, and can be considered as a complement to the review of Yanai and Wu (2006). Both the diagnosis and numerical experiments are used to get new insights into our understanding.

The remainder of this chapter is organized as follows. In section 2, there is an analysis of the relative importance of mechanical and thermal forcing induced by large-scale mountains. The diabatic heating characteristics of atmosphere over TP, the heating variability, and its impacts in winter are given in section 3. Section 4 focuses on how the mechanical forcing of the TP in late winter and early spring contributes to the occurrence of the persistent rainfall in early spring (PRES) over southern China and the early Asian monsoon onset. Section 5 discusses how large-scale topography affects the atmospheric vertical and horizontal circulations in summer based on idealized sensitivity experiments. Section 6 describes how the summertime continental forcing over Eurasia and the local forcing due to the TP work together to intensify the monsoon in East Asia and the dry climate in the Middle Asia, and how another plateau, the Iranian Plateau (IP), influences the Asian monsoon formation. Section 7 describes how the climbing and deflecting flow induced by topography influence the ASM and its configuration. A brief description of the change of the thermal forcing over the TP and a discussion on its impacts on the summer pattern of the eastern Asian precipitation are presented in section 8. Perspectives on future study are given in section 9.

2. Relative importance of mechanical and thermal forcing induced by large-scale mountains

The response of the atmospheric circulation to a thermal forcing could be considered as the response to a topography with a so-called equivalent mountain height H_Q (Held 1983), which is inversely proportional to the intensity of the basic flow u. For stationary waves forced by a zonal wavenumber-1 heating, Chen (2001) calculated H_Q corresponding to different zonal flows and found that H_Q is about 1 km for $u = 20\,\mathrm{m\,s^{-1}}$ and about 40 km for $u = 2\,\mathrm{m\,s^{-1}}$. For $u < 10\,\mathrm{m\,s^{-1}}$, the height of the equivalent topography is much larger than that of the real topography. Figure 7-1 shows the latitude–height cross section along 90°E of the climate-mean zonal wind in winter and summer months. In winter, the westerly jet of more than $40\,\mathrm{m\,s^{-1}}$ is just over the TP, whereas in summer the TP is located between easterlies to its south and westerlies to its north. These imply that mechanical forcing of the TP should be dominant in winter, whereas its heating is more important than topography in forcing the summer stationary waves in the subtropics.

a. Mechanical forcing

Figure 7-2 summarizes the linear atmospheric response to pure large-scale mechanical forcing (Wu 1984). For a

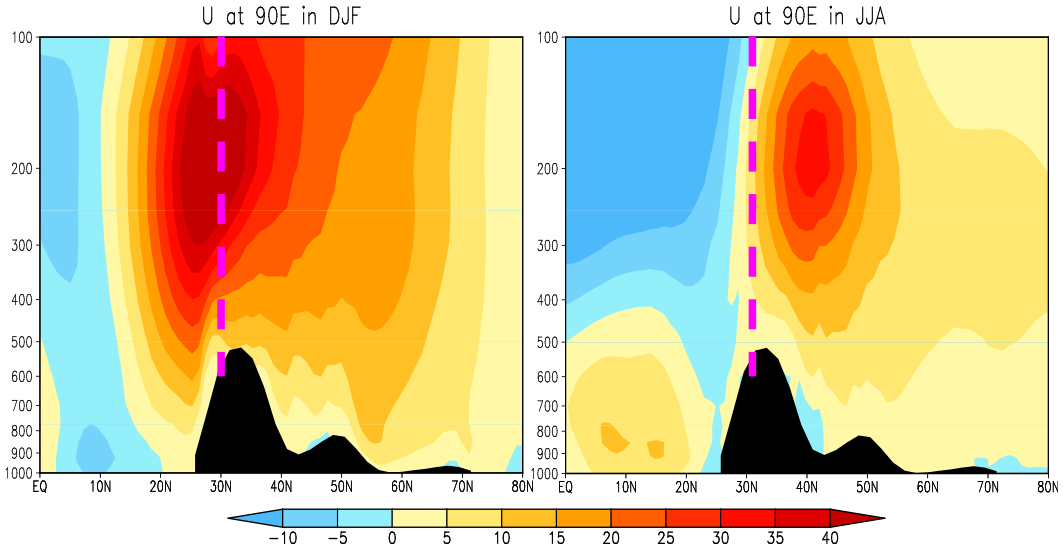

FIG. 7-1. Latitude–height cross section along 90°E of the climate-mean zonal wind (m s^{-1}) in (left) winter and (right) summer. The vertical dashed purple line shows the location of the TP.

barotropic atmosphere without friction, westerly flow climbing over a smaller (planetary scale) mountain will produce a ridge (trough) over the mountain ridge. The existence of friction always causes a ridge (trough) on the windward (lee) side of a mountain. For a baroclinic atmosphere without friction, westerly flow climbing over a smaller-scale mountain will produce a ridge over the mountain with its amplitude quickly decreasing

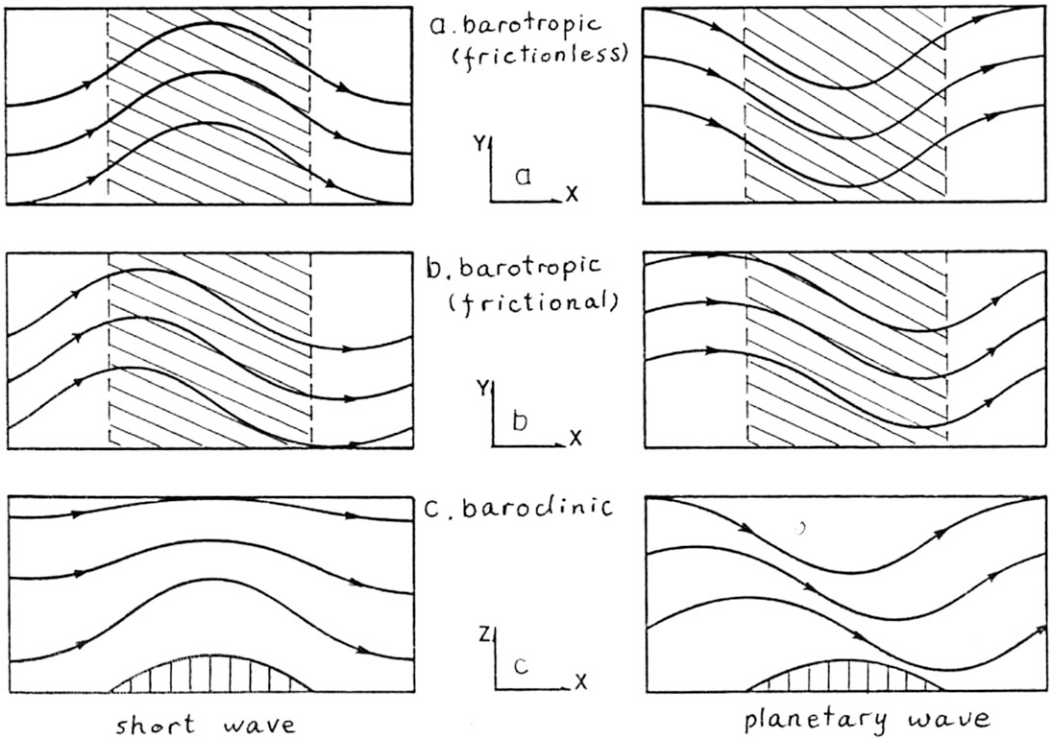

FIG. 7-2. Response of the atmosphere to large-scale mechanical forcing for different mountain scales under different atmospheric conditions for (left) short and (right) planetary waves: (a) frictionless barotropic, (b) frictional barotropic, and (c) baroclinic. The oblique lines in (a) and (b) and the vertical lines in (c) indicate where mountains are located [from Wu (1984)].

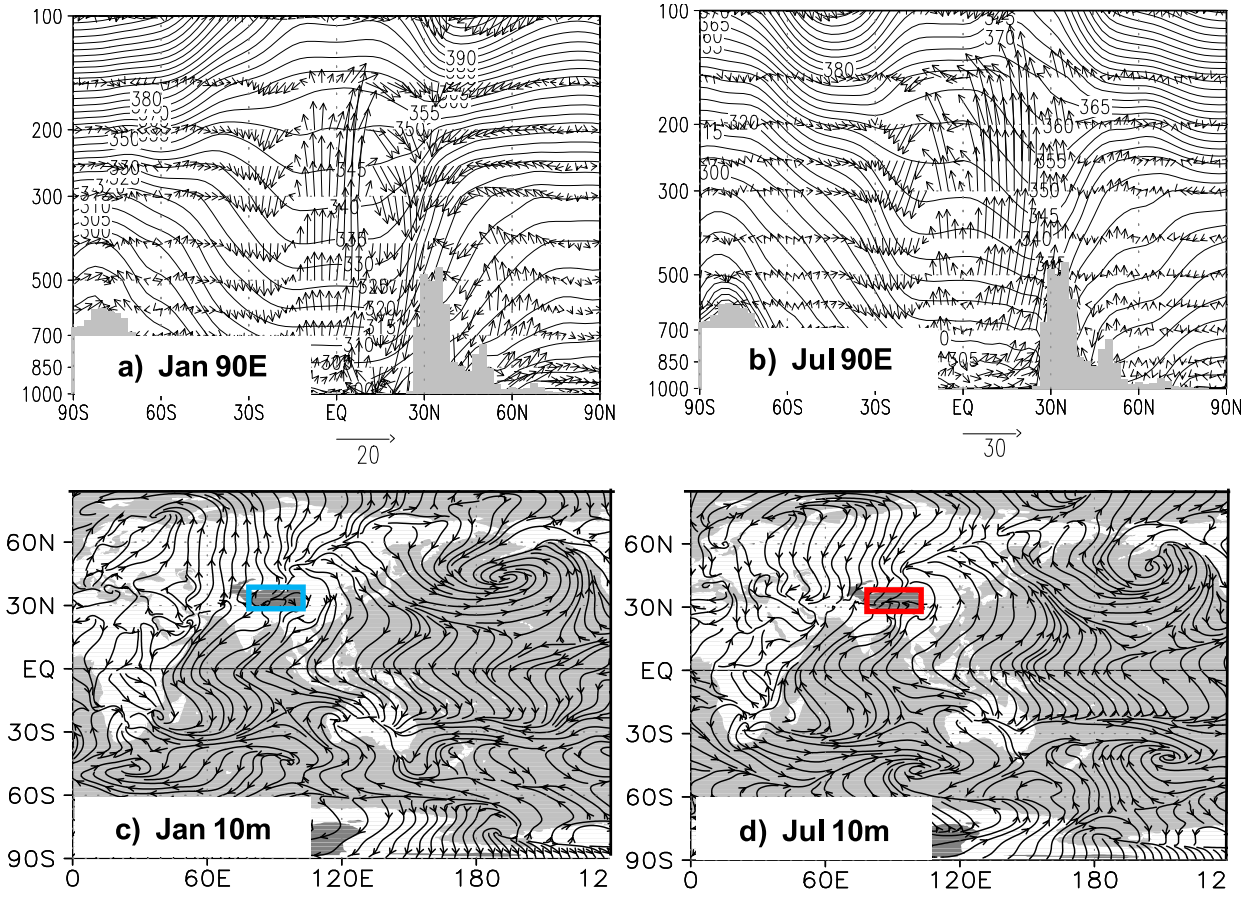

FIG. 7-3. TP-SHAP: The cross sections along 90°E of the (a) January and (b) July mean potential temperature (K) and circulation (vectors, m s^{-1}) projected on the cross sections. The deviations from the annual mean of the (c) January and (d) July mean streamlines at 10 m above the surface calculated from the NCEPII reanalysis for the period 1979–98. The blue box in (c) and the red box in (d) indicate the location of the TP [from Wu et al. (2007)].

vertically, whereas when climbing over a planetary-scale mountain, the flow will generate a westward tilting planetary mountain wave with wave energy propagating upward (Charney and Drazin 1961). On the other hand, the nonlinear atmospheric response to pure mechanical forcing can produce either climbing or deflecting flows depending on its height. Subjected to the constrains of energy and angular momentum conservations, a critical mountain height H_c, which is from about several hundred to one thousand meters, can be derived (Wu 1984). If the height of a mountain is higher than H_c, airflow impinging upon a mountain will be deflected around the mountain, whereas for a mountain lower than H_c, airflow can climb over and produce air descent on the lee side.

b. Thermal forcing: TP sensible heat–driven air pump

Figures 7-3a and 7-3b show the cross sections along 90°E of the monthly mean potential temperature and wind vector projected on the cross sections for January and July, respectively, in which the vertical velocity w has been multiplied by 10^3. In January, cold temperatures over continental areas and warm temperatures over ocean are prominent. Atmospheric cooling indicated by air descent ($\mathbf{V} \cdot \nabla\theta < 0$) prevails in the free troposphere over continents. The strongest cooling is over the TP and its southern slope, with the strong heating and ascent over the equator in contrast. During summer, the warmest center of potential temperature is just above the TP. This is in agreement with the existence of the warm temperature center in July over the plateau (Yanai et al. 1992). Strong ascent prevails in the area from east of the TP to eastern China (figure not shown) and to its south from the TP to the Bay of Bengal (BOB) (Fig. 7-3b), penetrating the isentropic surfaces upward almost perpendicularly and indicating the existence of a strong heating source over the area in summer. Figures 7-3c and 7-3d show, respectively, the deviations from the annual mean of the January-mean

and July-mean streamlines 10 m above the surface calculated from the NCEP-II reanalysis for the period 1979–98. It is evident that deviating air currents flow from the winter hemisphere into the summer hemisphere, diverging out of continents and converging toward oceans in midlatitude areas in the winter hemisphere, but converging toward the continents and diverging out of oceans in the summer hemisphere. A remarkable circulation reversal appears over the Asian–Australian (A–A) monsoon area. In January the surface air diverges out of the TP region toward South Africa and Australia, whereas in July the surface air is converged into the TP region from South Africa and Australia, characterizing the seasonal reversal of the A–A monsoon flows.

In summary, cold and dry air in winter descends over the TP then diverges toward the surrounding areas, whereas in summer moist and warm air converges from the surroundings, particularly from the Indian and western Pacific Oceans, toward the TP region where it is uplifted to the free atmosphere to form cloud and monsoon precipitation. The whole process repeats from year to year and acts like a huge air pump. Since the work done by the air pump is basically driven by the surface sensible heating of the TP, it was named the TP sensible heat–driven air pump (TP-SHAP).

c. TP-forced stationary waves and the associated climate

Figure 7-4 depicts the winter- and summer-mean distributions of potential temperatures and the stream field composed of zonal deviation winds at 850 hPa. In winter months the topography retards the impinging midlatitude winds and deflects the westerly from zonal to circumcolumnar flow (Fig. 7-4a). The deviation streamlines depict an asymmetric dipole shape with an anticyclone to the north of the TP and a cyclone to its south. The streamlines then converge over eastern China and go into its eastern pole but come out of its western pole and diverge over central Asia. The anticyclonic deviation circulation gyre in high latitudes transports warm air northward to its west but cold air southward to its east. As a result, the isotherms in the high latitudes of Asia tilt from northwest to southeast, and the temperature at 130°E is colder than that at 50°E by 10 K at 40°N and 14 K at 50°N. On the other hand, the cyclonic deviation circulation gyre in low latitudes transports dry air southward to South Asia subcontinent, but moist air northward to the Indochina Peninsula and southern China. As a result, a prolonged dry season in South Asia and persistent rainy season in Southeast Asia and southern China are observed before the Asian monsoon onset. In the summer months, the strong TP heating excites a huge cyclonic deviation circulation over East

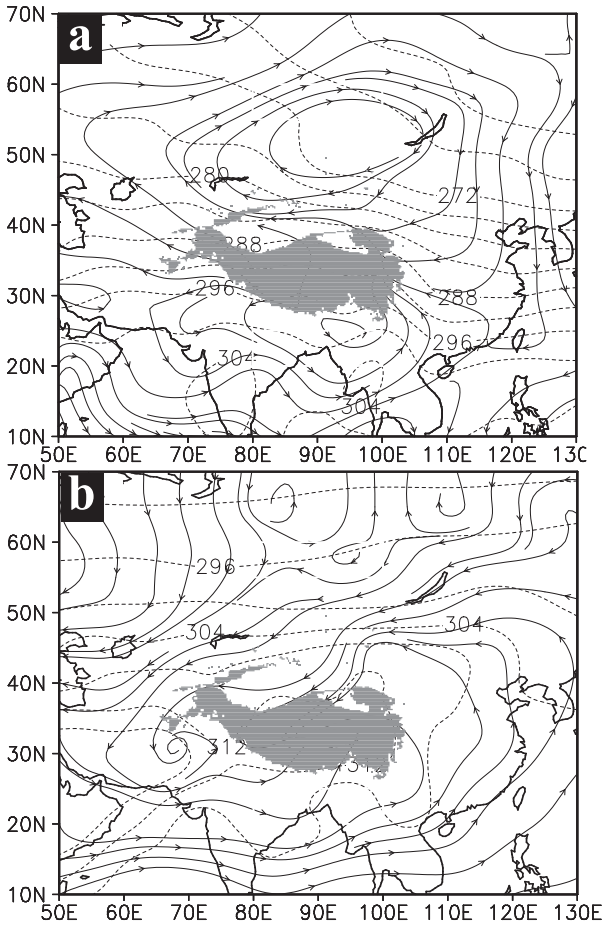

FIG. 7-4. Distributions at 850-hPa potential temperature (dashed lines; K) and the stream fields (lines with arrows) composed of wind deviations from the corresponding zonal means based on the NCEP–NCAR reanalysis for 1968–97. (a) Winter average between December and February. (b) Summer average between June and August [from Wu et al. (2007)].

Asia, and the strong pumping of the TP-SHAP makes the surrounding flows converge into the TP area. Therefore, the summer pattern of the deviation stream field at 850 hPa resembles a huge cyclonic spiral and the TP-SHAP looks like a spiral pump. In fact, the summer TP is an important genesis location of vortices that can propagate eastward and result in torrential rain along the Yangtze River.

3. Thermal characteristics over the TP in winter and their implications

There are three kinds of atmospheric diabatic heating: diffusive sensible heating including surface sensible heating; condensation latent heating, including both large-scale condensation heating and deep convection condensation heating; and radiative heating, which

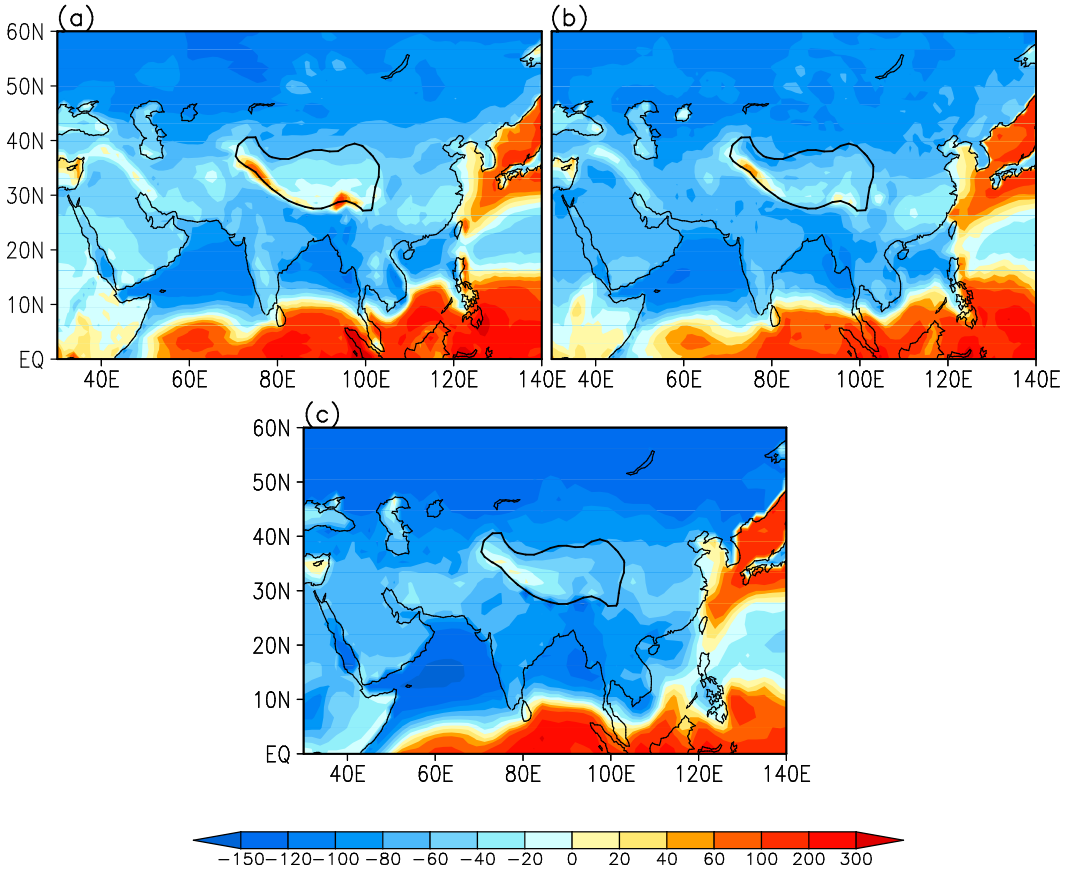

FIG. 7-5. Distribution of climatological-mean total column-integrated diabatic heating ($W\,m^{-2}$) in winter (December–February; the 3000 m orographic height is depicted by the bold black contour): (a) ERA-40, (b) JRA-25, and (c) NCEP2 [from Yu et al. (2011a)].

includes positive shortwave radiative heating and negative longwave radiative cooling. Usually the heating data in reanalyses are not as reliable as those of the temperature and wind. However, such heating data from ECMWF and NCEP have been gauged by the extent of their dynamical consistency with the large-scale circulation and it was shown that they are reasonably consistent estimates (Nigam 1994, 1997). Here we will use the above three kinds of heating to investigate the thermal status over the TP.

a. Climatology of the TP thermal status

The diabatic heating characteristics of the atmosphere over the TP in wintertime was analyzed by using three kinds of reanalysis data of diabatic heating. The strong column-integrated heating is observed over the southwestern flank of the TP, equatorial Indian Ocean, and western Pacific as well as the storm track regions over the northwestern Pacific in winter (Fig. 7-5). They are predominantly due to condensational latent heat release that accompanies the precipitation when westerly climbs up the TP, the ITCZ rains and the storm precipitation (Figs. 7-6a,b), and to strong surface sensible heating (Figs. 7-6c,d) from warmer ocean to the east coast of China. There is diabatic cooling over the Asian continent and tropical Indian Ocean and South China Sea (Fig. 7-5). The stronger cooling in high latitudes results from the remarkable surface cooling (Figs. 7-6c,d), and weaker solar radiation (Figs. 7-6g,h), whereas the cooling over the north Indian Ocean is mainly caused by the stronger longwave radiation (Figs. 7-6e,f). Although there are some quantitative differences among different reanalysis data, three kinds of diabatic heating data basically yield similar climatological distributions (Yu et al. 2011a).

b. Interannual variation of wintertime diabatic heating and its impacts

EOF analysis shows that the leading mode (EOF1) of interannual variation of the total column-integrated diabatic heating in January over the TP shows the most remarkable variation of the diabatic heating concentrates

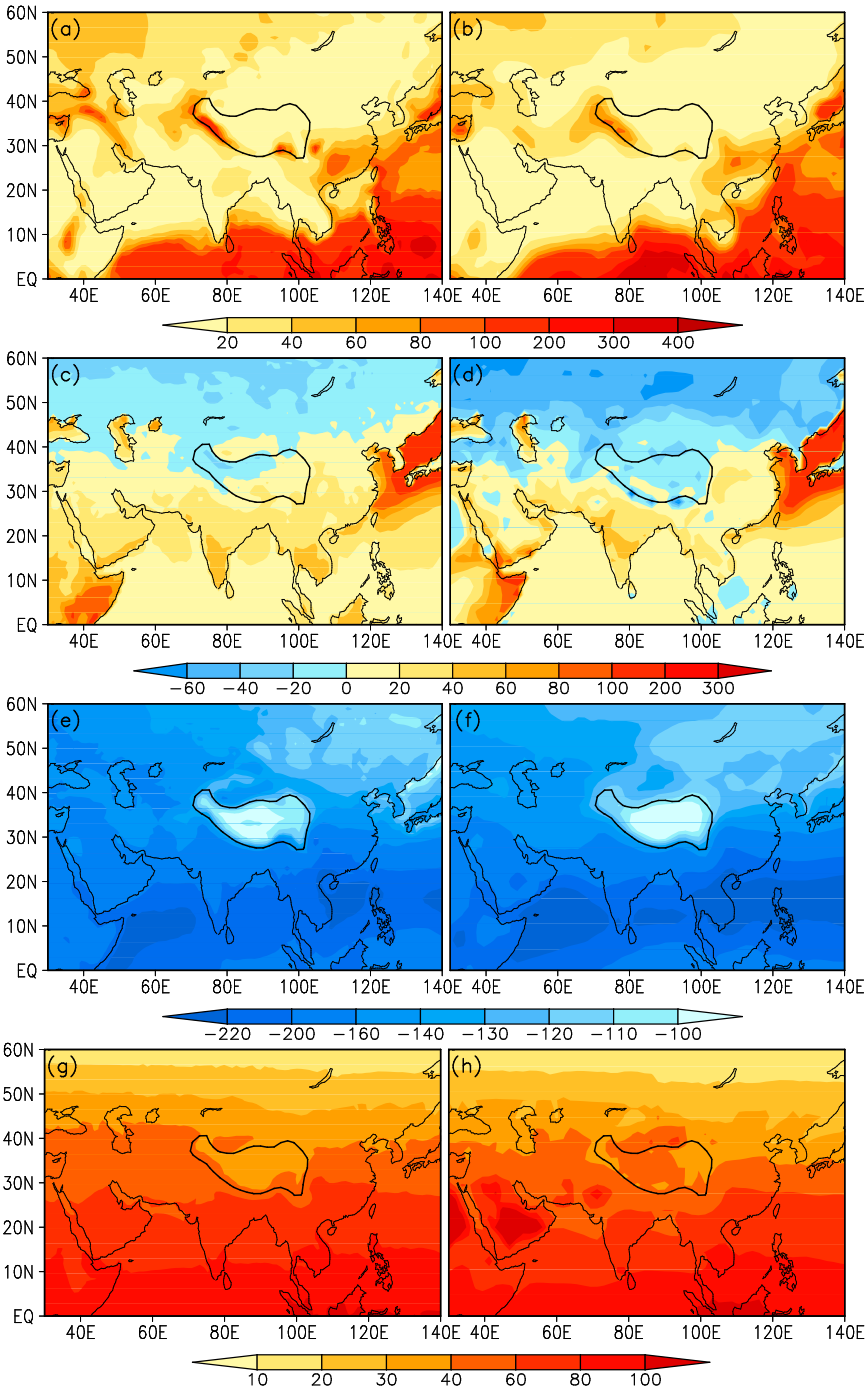

FIG. 7-6. Distribution of climatological mean column-integrated diabatic heating component in winter ($W\,m^{-2}$): (a),(b) latent heating, (c),(d) sensible heating, (e),(f) longwave radiative heating, and (g),(h) shortwave radiative heating, from (left) JRA-25 and (right) NCEP2 [from Yu et al. (2011a)].

on its west and southeast (Fig. 7-7), a pattern fairly close to that of the climate-mean total heating as shown in Fig. 7-5. The three reanalysis datasets produce similar spatial and temporal variation of the heating. Data diagnosis and numerical modeling indicate that the interannual variation of this heating is closely related with the corresponding upstream westerly, just to the southwest side of the TP. Because circulation data are more

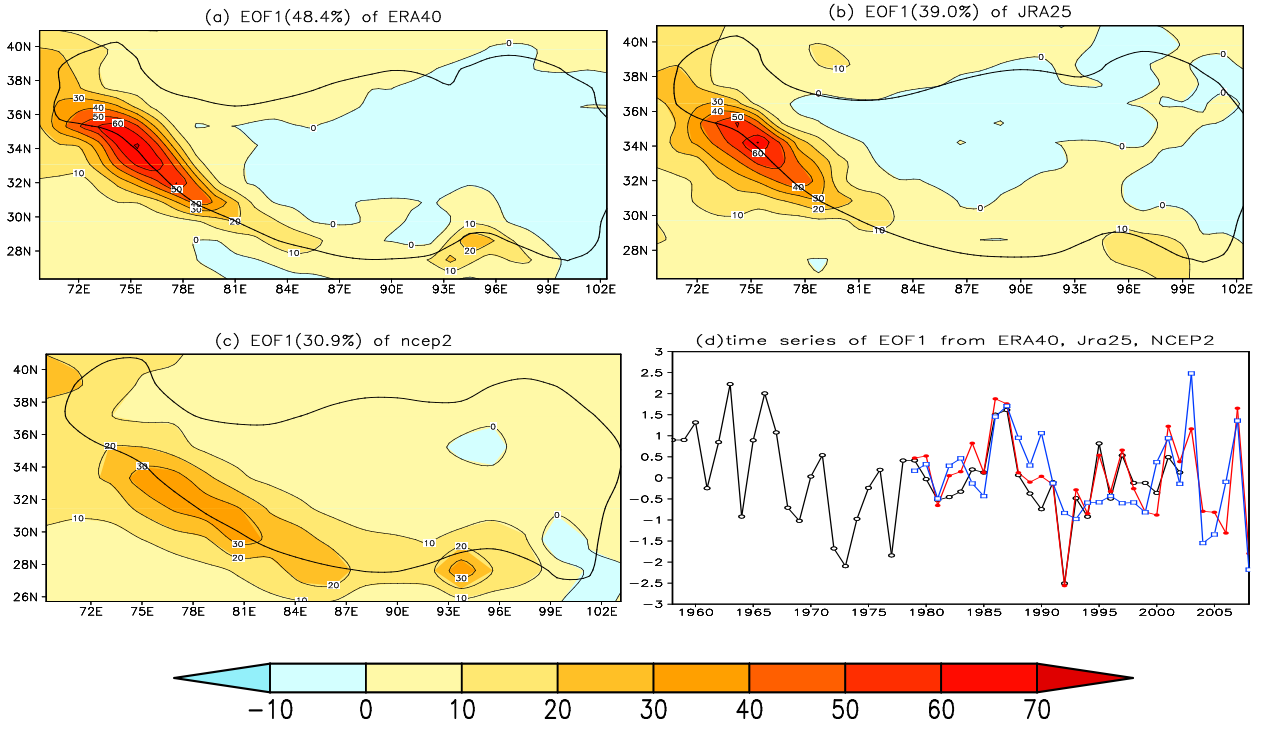

FIG. 7-7. Distribution of main interannual variation mode (EOF1) of total column-integrated diabatic heating (W m^{-2}) in January over the TP (the orographic height of 3000 m is depicted by the black contour) from analysis of (a) ERA-40 (1958–2002), (b) JRA-25 (1979–2008), and (c) NCEP (1979–2008) [from Yu et al. (2011b)]. (d) The corresponding PCs; black, red, and blue curves are for ERA-40, JRA-25, and NCEP, respectively.

reliable compared with diabatic heating data, a westerly index (the West Index) representing the TP heating status is thus defined as the mean westerly at 700 hPa averaged over the upstream region (20°–30°N, 40°–70°E) (Yu et al. 2011b). The West Index is then used to identify the circulation associated with the TP heating variation. Figure 7-8 demonstrates the regression of the West Index with circulations in different layers. Different from summer, there appear consistent cyclonic (or anticyclonic) anomalous circulations over the TP from the lower troposphere to the upper troposphere when the column-integrated diabatic heating over the TP is above (or below) normal, demonstrating an equivalent-barotropic abnormal structure (Figs. 7-8a–c). When the upstream westerly to the southwest of the TP is getting stronger, cyclonic anomalous circulation in the northwest of TP develops due to topography blocking, the detouring flow around the south side of TP becomes stronger, and the cyclonic anomalous circulation around TP also develops (Yu et al. 2011b). Consequently, these lead to the increase of precipitation, latent heating, and total heating over the west and southeast of the TP. It becomes apparent that the abnormality of diabatic heating in winter over the TP is the result of atmospheric circulation abnormality and the mechanical effect of TP. It is demonstrated that the heating over the TP in winter is a local response to a specific abnormal mode of atmospheric circulation in the Northern Hemisphere, which is closely related with the teleconnection wave pattern oriented from northwest to southeast in the Northern Hemisphere. Nevertheless, the diabatic heating anomalies over the Tibetan Plateau was reported to be closely related to the extreme heavy snow and cold event in January 2008 over southern China as shown in Fig. 7-8d (Bao et al. 2010; Li et al. 2011).

4. TP forcing in spring and Asian summer monsoon onset

a. Persistent rains in early spring over southern China

Besides the well-known Asian monsoon, another less-known unique feature of Asian rainfall is the occurrence of persistent rains in early spring (PRES) over southern China. From late February to early May (pentads 12–26) before the onset of the Asian monsoon, persistent rains occur over a large area south of the Yangtze River. However, the formation mechanism is still unclear. Tian and Yasunari (1998) proposed a mechanism of time lag in the spring warming between land and sea to explain

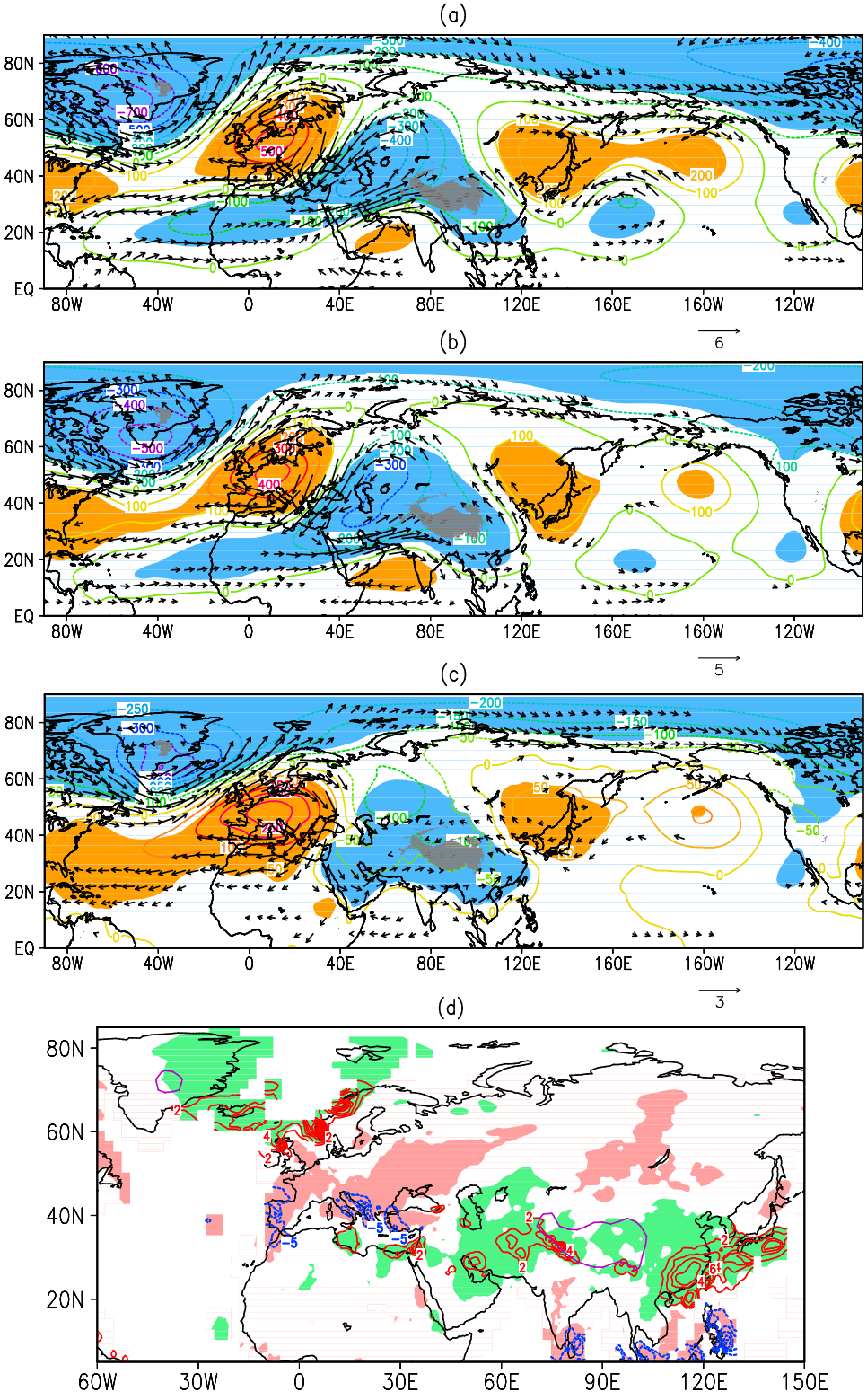

FIG. 7-8. Wind vectors (statistically exceeding 95% confidence; m s^{-1}) and height field (contours; Pa) at (a) 200, (b) 500, and (c) 850 hPa. (d) Land precipitation regressed on the West Index from ERA-40 [contours with red (blue) are positive (negative); shading indicates correlation coefficients statistically exceeding 95% confidence. In (a)–(c) orange (blue) shading shows positive (negative) correlation; in (d) green (red) shading shows positive (negative) correlation [from Yu et al. (2011b)].

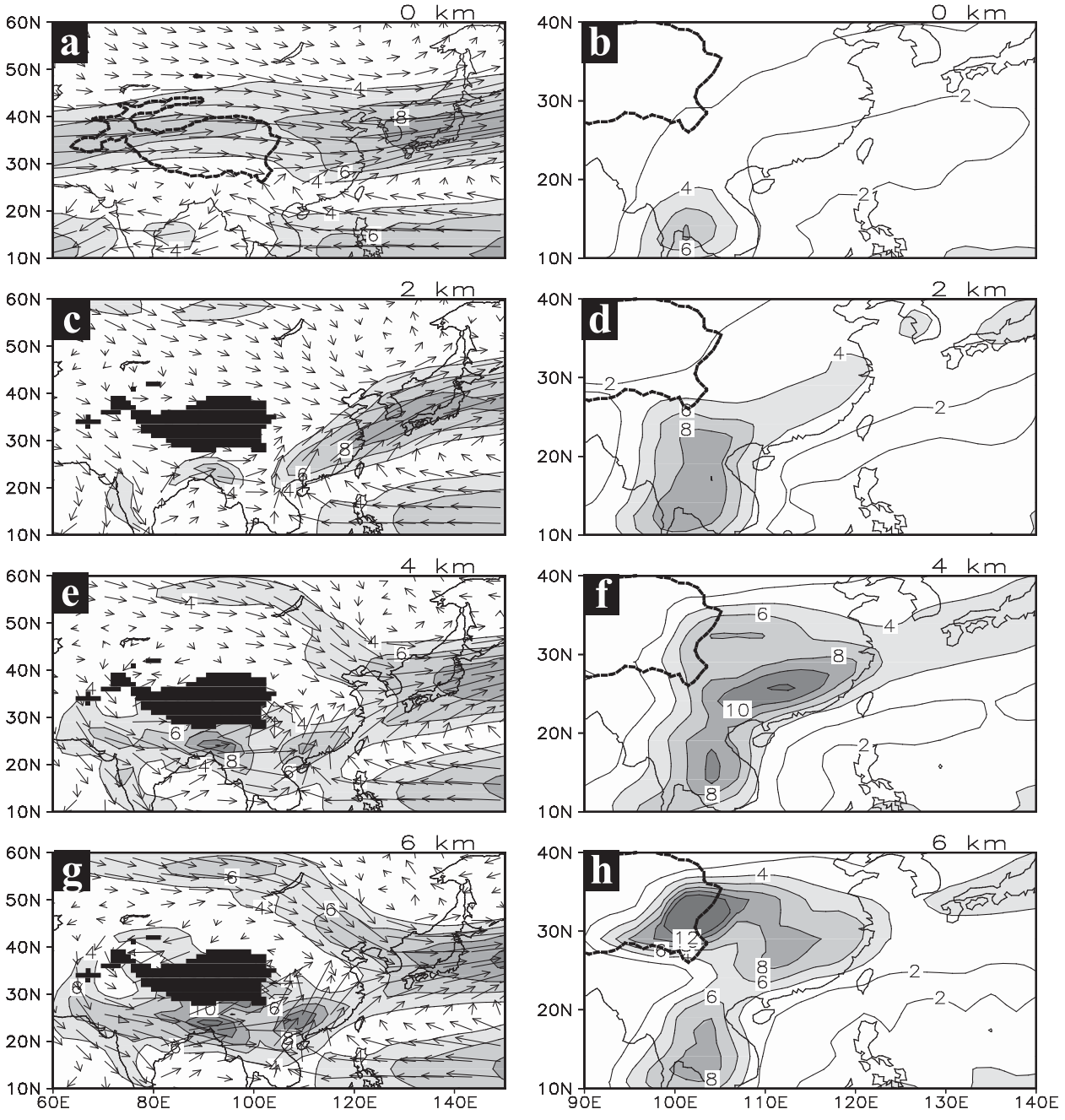

FIG. 7-9. Distributions of (a),(c),(e),(g) wind vectors and isotachs at 850 hPa (m s^{-1}; shading indicates >4 m s^{-1}) and (b),(d),(f),(h) rain (mm day^{-1}) in the perpetual spring sensitivity experiments with (top to bottom) different TP elevations and averaged over 30 months. The black shading in the left panels and the bolder solid curve in the right panels are the main part of TP. The TP maximum elevation is 0 km in (a),(b), 2 km in (c),(d), 4 km in (e),(f), and 6 km in (g),(h) [from Wan and Wu (2007)].

the formation of the PRES. However, a recent study of Wan and Wu (2007) shows that such a heating time-lag mechanism also exists between Mexico and the western North Atlantic in the same period, but there is no PRES in North America. It turns out that the time-lag mechanism is a necessary condition but not sufficient for the occurrence of the PRES.

As demonstrated in Fig. 7-4a, before the monsoon onset the TP can generate a dipole-type stationary circulation pattern. The deflected flow brings cold air from the north and moist air from south, which then converge over eastern China. This may contribute to the formation of PRES. To verify this hypothesis, a series of numerical experiments were conducted by Wan and Wu (2007) and

Wu et al. (2007). To focus on physical mechanisms, perpetual April integrations are designed in the following experiments. The solar angle is set to 10 April. Figure 7-9 shows the wind vector at 850 hPa and rainfall in the experiments when the elevation of the TP is leveled at 0, 2, 4, and 6 km, respectively (Wu et al. 2007).

In the ''no TP'' experiment, the westerly jet in Eurasia does not split, and a zonally oriented subtropical anticyclone belt dominates in the middle to low latitudes (Fig. 7-9a). Significant rainfall appears only in the southwest of the Indochina Peninsula, in association with the easterly perturbation forced by land–sea thermal contrast (Fig. 7-9b). After the elevation of the TP reaches 2 km, the westerly jet starts to split into its northern and southern branches (Fig. 7-9c). They meet downstream of the TP, forming a strong Asian jet. The belt of subtropical anticyclone breaks, and a prominent anticyclonic center appears over the western Pacific. Therefore the distribution of rainfall takes the shape of PRES (Fig. 7-9d). In the 4-km TP experiment, the split westerly jets on both north and south sides of the TP are strengthened, the circulation pattern (Fig. 7-9e) is already close to the simulation counterpart in the control simulation in which the seasonal variation is included (Wu et al. 2007), and the PRES appears (Fig. 7-9f). In the 6-km TP experiment, the wintertime TP dipole circulation becomes stronger compared to the control simulation. As a result, the PRES is weakened, and the main rainfall center moves to the eastern TP (Fig. 7-9h) where the convergent entrance pole of the TP dipole in the wintertime deviation streamline pattern is located.

The above experiments prove that PRES are formed efficiently due to the deflecting effects of the TP. When the deflected flow—the cold air from the north and the warm and moist air from the south—meet downstream of the TP PRES are formed. The experiments further demonstrate that the intensity and location of the PRES are to some extent influenced by the elevation of the TP.

b. Asian summer monsoon onset

Wu and Zhang (1998) showed that it is due to mechanical as well as thermal forcing of the TP that the onset of the Asian summer monsoon is composed of three consequential stages. The earliest is over the region from the eastern BOB to the western Indochina Peninsula in early May. The Bay of Bengal monsoon onset creates favorable conditions for the South China Sea (SCS) monsoon onset in mid-May (Liu et al. 2002b). This leads to great changes in both large-scale circulation and diabatic heating over Asia. Finally, the onset of the Indian monsoon appears in early June. Since then, many studies have been conducted to determine the underlying mechanism. A numerical simulation based on idealized land–sea distribution developed by Liang et al. (2005) proved that TP heating in late spring greatly intensifies the southern branch of the wintertime dipole of the 850-hPa stream field. This intensified southern branch of the dipole enhances the southerlies to the southeast of Tibet and brings heavy rainfall and more latent heating over the eastern Bay of Bengal and to its east, resulting in Asian summer monsoon onset over the eastern BOB (Fig. 7-10a). It also produces prevailing northerlies to the southwest of Tibet, resulting in less rainfall and more sensible heating over the Indian subcontinent. If the TP is moved westward by 30° in longitude to the north of the Arabian Sea, then the onset site of the Asian monsoon is also moved westward by 30° (Fig. 7-10b). It is evident that the TP anchors the onset site of the Asian summer monsoon to a place over the eastern BOB, just to the southeast of the TP. It is also found that stronger surface sensible heating on the TP in spring leads to an earlier seasonal transition in eastern Asia (Duan and Wu 2005; Mao and Duan 2005).

Commonly, in the lower troposphere the monsoon onset is preceded by the development of a monsoon onset vortex (MOV) (Krishnamurti 1981). The northward moving of the onset vortex can lead to the break of the ridgeline of subtropical anticyclone over the eastern BOB region in the lower troposphere and activate the India–Burma trough, resulting in the BOB summer monsoon onset. Case studies (Wu et al. 2011, 2012a) demonstrate that the formation of the BOB monsoon onset vortex is a consequence of in situ air–sea interaction modulated by the land–sea thermal contrast in South Asia and TP forcing in spring, which can be interpreted schematically by Fig. 7-11: in spring the dominant cold northwesterly over India that is induced by the TP forcing generates strong surface sensible heating and cyclonic circulation. The resultant southwesterly over the northwestern BOB together with the seasonal near-equator westerly forms a steady anticyclone circulation to the north of the BOB and cyclone circulation to its south (Fig. 7-11a) and produces offshore ocean current as well as upwelling in the western BOB. Warm surface water is transported eastward and accumulated on the eastern BOB (Fig. 7-11b). More importantly, the strong downward shortwave radiation over the northern BOB under the anticyclone condition heats the surface water with a thin thermocline of less than 20 m and the SST rises fast over the central and northeastern BOB, forming a strong spring BOB warm pool there (Figs. 7-11b,c). On the southern rim of the warm pool, stronger surface sensible heating from ocean to atmosphere is produced because of the development of the near-equator westerly (Fig. 7-11c), where temperature and heating are positively correlated and

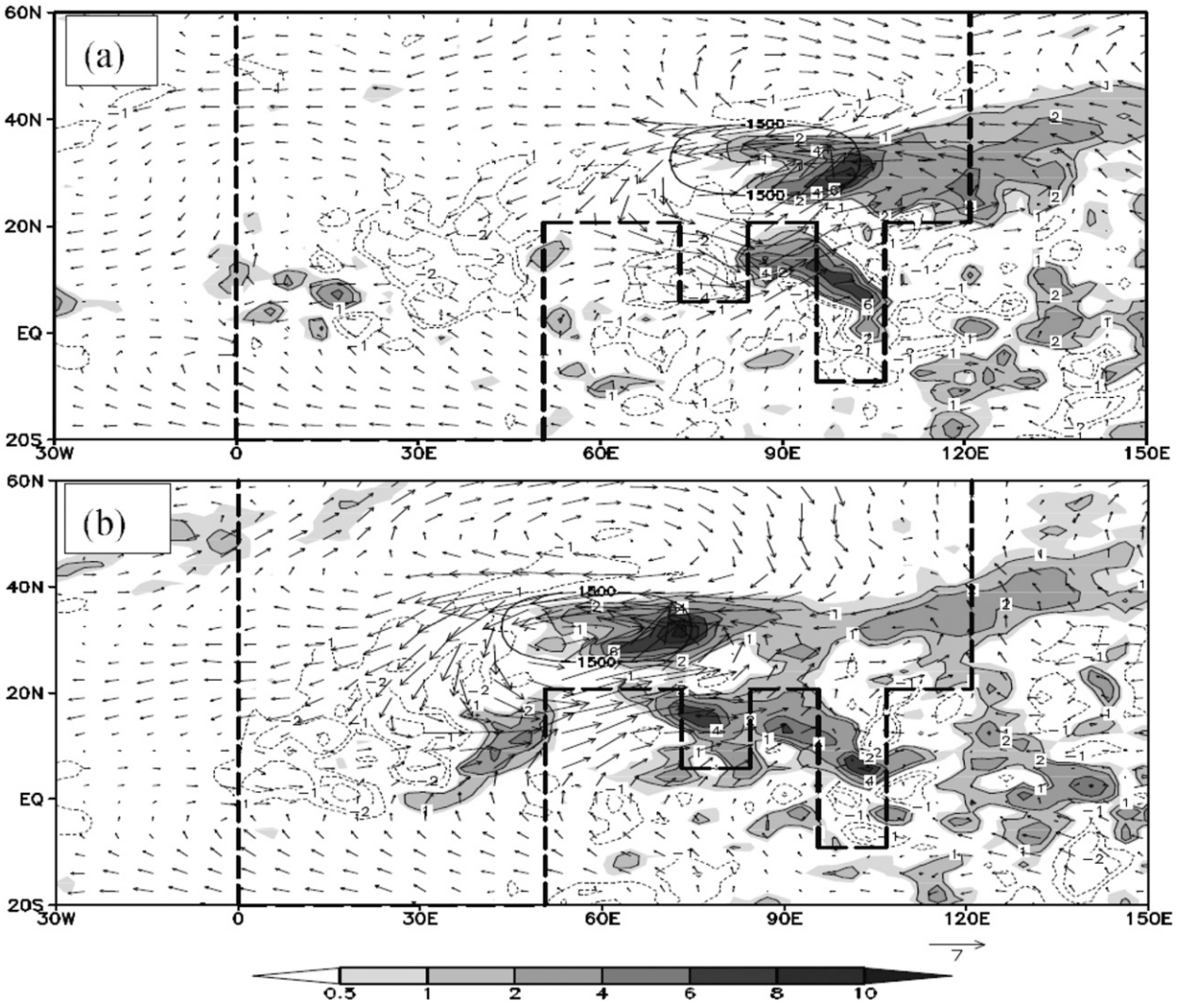

FIG. 7-10. Differences in precipitation (mm day^{-1}; shading) and wind vectors (m s^{-1}) at 850 hPa with and without TP experiments during the Asian summer monsoon onset time. The virtual TP is centered at (a) 33°N, 90°E and (b) 33°N, 60°E by using the GOALS-SAMIL model. The heavy dashed line denotes the continent boundary. [Adapted from Liang et al. (2005).]

atmospheric available energy is generated, thus favoring of the development of monsoon onset vortex over the southern BOB.

In spring, the zonal westerly just crosses the TP. Then because of the strong zonal advection the TP heating in late spring generates cold (warm) air temperatures upstream (downstream) of the TP. This can stimulate the summer-type meridional temperature gradient in the upper troposphere (cold in south and warm in north) to the east of the TP and enhance the winter-type meridional temperature gradient in the upper troposphere (cold in north and warm in south) to its west, providing a favorable background to the east of the BOB for summer monsoon onset to follow (Wu and Zhang 1998). More importantly, the significant latent heat release due to the BOB monsoon generates a stationary Rossby wave train in the middle and upper troposphere with an anticyclone circulation over southern China, bringing colder air southward to the southern coast of China to meet the northward transported warm and moist air, which is brought about by transient eddies exited by the BOB monsoon latent heating as well (Liu et al. 2002). Consequently, the SCS summer monsoon onset commences.

The huge latent heating released by the BOB and SCS monsoon stimulates the unstable development of the South Asian high (SAH) in the upper troposphere, which extends westward with a remarkable divergence developing on its southwest just above the southeastern coast of Arabian Sea, forming a local and strong upper

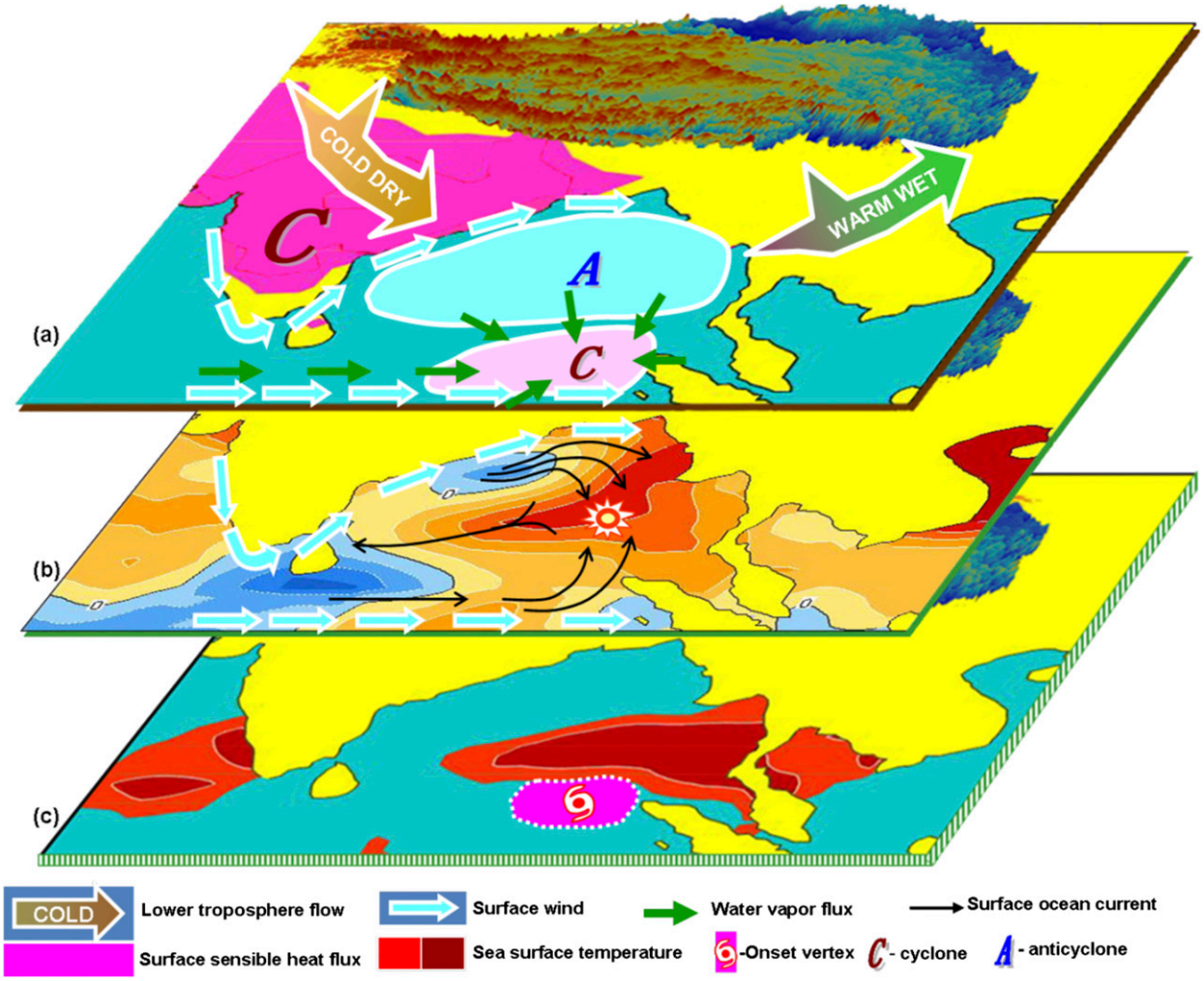

FIG. 7-11. Schematic diagram showing the formation of the BOB monsoon onset vortex as a consequence of in situ air–sea interaction modulated by the land–sea thermal contrast in South Asia and TP forcing in spring. See the text for details [from Wu et al. (2012a)].

layer pumping. Indian summer monsoon is induced at last (Zhang et al. 2014).

It becomes clear that the TP forcing in late spring can control the progression of the Asian summer monsoon onset.

5. Topography impacts on regional circulation and ASM

a. Topography impacts on regional circulation

Figure 7-3 demonstrates that the TP-SHAP plays significant roles in regulating the Asian monsoon climate. However, it is not clear whether the removal of surface sensible heating especially on the sloping surfaces will suppress the convergence (divergence) of the surface air flows from (into) the surrounding areas in the lower layers. To illustrate the significance of the sensible heating over the sloping surfaces in the operation of the TP air pump, a series of aquaplanet experiments have been conducted based on an atmospheric general circulation model FGOALS_s developed at LASG, Institute of Atmospheric Physics (IAP). For the present purpose, aquaplanet experiments are designed with an idealized topography being introduced into the aquaplanet in which Earth's surface in the model is covered merely by ocean. There are four experiments (Fig. 7-12) (Wu et al. 2007):

1) ALLSH: All of the virtual TP surfaces possess surface sensible heating;
2) SLPSH: Only the sloping TP surface possesses surface sensible heating;
3) TOPSH: Only the top TP surface possesses surface sensible heating; and
4) NOSH: None of the TP surfaces possesses surface sensible heating.

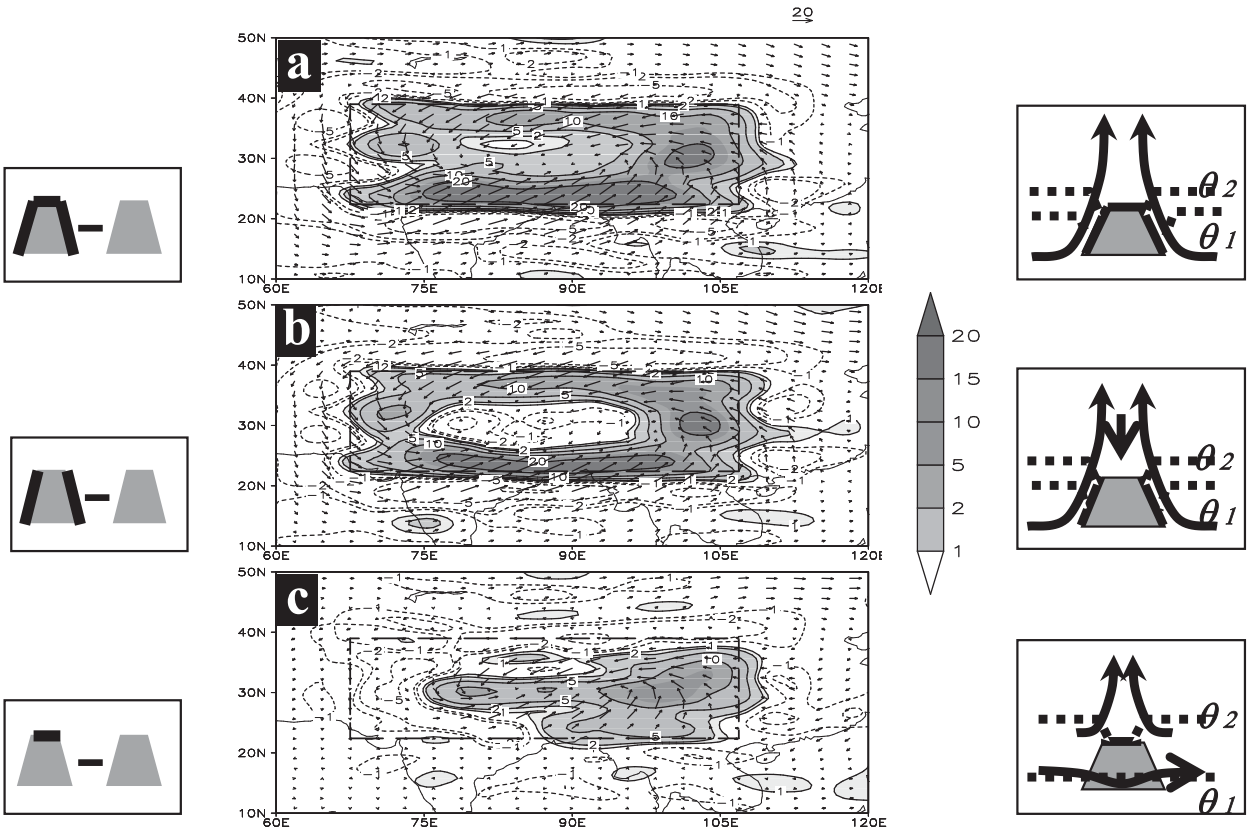

FIG. 7-12. Distributions of the wind difference (vectors) and vertical velocity ($-\omega$, shading, 10^{-2} Pa s^{-1}) on the $\sigma = 0.991$ surface from the perpetual July experiments (a) ALLSH-NOSH, (b) SLPSH-NOSH, and (c) TOPSH-NOSH, for (left) experiment designs and (right) mechanism interpretations [from Wu et al. (2007)]. The dashed line denotes the continent boundary [from Wu et al. (2012b)].

In constructing all the "no sensible heat" cases, the diffusive heating term in the atmospheric thermodynamic equation is set to zero while the surface sensible heating from the surface continues to release. Therefore, the surface energy balance is maintained. Then the differences between the three pairs (i.e., ALLSH–NOSH, SLPSH–NOSH, and TOPSH–NOSH) can be considered, respectively, as the impacts on the circulation of the TP due to all surface sensible heating, sloping-surface sensible heating alone, and top-surface sensible heating alone. Their differences in horizontal wind and vertical motion at the lower model level $\sigma = 0.991$ are presented in Fig. 7-12. Coastlines are added into the figure only for reference and comparison. In the all-surface sensible heating case (Fig. 7-12a), surface air from the Arabian Sea, Indian subcontinent, BOB, Indochina Peninsula, and the other neighboring areas are converged into the TP area and ascend over the TP. The enhanced upward movement of more than -0.2 Pa s^{-1} is on its southern and eastern slopes where the release of latent heating further intensifies the ascent. The sloping-surface sensible heating produces similar circulations (Fig. 7-12b) as in the case with the surface sensible heating impose on all the TP surfaces (Fig. 7-12a) except over the platform: because of the absence of the in situ surface sensible heating, air descends over its top in association with radiation cooling. On the other hand, the mere top-surface sensible heating produces convergence flow only above the platform where the elevation is already higher than 3 km (Fig. 7-12c). There is no convergence at the lower elevations, and the main ascent appears over the eastern TP as a stationary Rossby wave response to the top surface heating. The results shown above can be explained by the right panels in Fig. 7-12. In the presence of surface sensible heating on the sloping surfaces (Figs. 7-12a,b), the heated air particles at the sloping surface penetrate the isentropic surfaces and slide upward. The air in the lower elevation layers in the surrounding areas is therefore pulled into the plateau region, forming strong rising motion and even heavy rainfall over the TP. On the contrary, in the top-heating-only case (Fig. 7-12c), although the platform

heating can result in air convergence above the plateau it cannot pull air from below. This is because when an air particle is traveling in the lower layer and impinging on the TP, it has to stay at the same isentropic surface because of the absence of diabatic heating from the sloping lateral surface of the TP. Therefore, the air particle just goes around the TP at a rather horizontally located θ surface and no apparent ascent occurs. Therefore, there are no significant impacts on monsoon rainfall. It becomes evident that such an air pump is driven by the surface sensible heating on the TP (the TP-SHAP).

b. Topography impacts on ASM

The general circulation model FGOALS_s was used again to conduct idealized experiments for understanding the roles of large-scale mountains in the Asian summer monsoon. Three experiments, Exp TRO, Exp TP, and Exp IPTP, are designed to investigate the influence on Asian monsoon of the TP and Iranian Plateau in which idealized land–sea distribution and orography are used (Wu et al. 2012b):

(a) Exp TRO, the main Eurasian continent located over 20°–90°N, 0°–120°E and three square-shaped tropical lands over 35°S–20°N, 0°–50°E; 5°–20°N, 75°–85°E; and 9°S–20°N, 95°–105°E are integrated to form the "Afro-Eurasian continent."
(b) Exp TP, an idealized TP with the following ellipsoidal shape is placed on the continent in Exp TRO:

$$h(\lambda,\varphi) = h_{\max}\cos\left(\frac{\pi}{2}\frac{\lambda-\lambda_0}{\lambda_d}\right)\cos\left(\frac{\pi}{2}\frac{\varphi-\varphi_0}{\varphi_d}\right),$$

where $(\lambda_0, \varphi_0), (\lambda_d, \varphi_d)$, and $h_{\max}$ are taken at (32.5°N, 87.5°E), (8.25°N, 25.0°E), and 5 km.
(c) Exp IPTP, an idealized IP, where $(\lambda_0, \varphi_0), (\lambda_d, \varphi_d)$, and $h_{\max}$ are set at (32.5°N, 53.4°E), (8.25°N, 22.5°E) and 3 km, is added to Exp TP.

Figure 7-13a shows the simulated distributions of precipitation and the wind field in July at the near-surface level $\sigma = 0.991$ in Exp TP. Figure 7-13b shows the differences between the experiments with and without the TP. The elevated mountain heating produces not only lower-troposphere cyclonic circulation but also strong rainfall ($>16\,\text{mm day}^{-1}$) on the southeastern slope of the TP, partly because the local sensible heating generates a geostrophic Rossby wave with air ascent to the east and descent to the west, and partly because over the southeastern TP the upstream warm, moist air that is transported along the southwesterly from the Indian Ocean is pumped upward. The TP acts to enhance the coupling between the lower and upper tropospheric circulations and between the subtropical and tropical monsoon circulations (Fig. 7-14), resulting in an intensification of the East Asian summer monsoon and a weakening of the South Asian summer monsoon (Fig. 7-13b). Linking the Iranian Plateau to the TP substantially reduces the precipitation over Africa and increases the precipitation over the Arabian Sea and the northern Indian subcontinent, effectively contributing to the development of the South Asian summer monsoon (Figs. 7-13c–e).

6. Thermal control of the Asian summer monsoon

The relative impacts of various land–sea distributions (LSDs) and mountains on Asian monsoon extent and intensity have been assessed by Xu et al. (2009, 2010a,b) based on a series of AGCM simulations. Their results indicate that the presence of a midlatitude zonal LSD induces a strong zonal pressure gradient between the continent and ocean, which in turn results in the formation of an East Asian subtropical monsoon. The presence of the Asian mountains results in a stronger South Asian summer monsoon (SASM), as well as East Asian summer monsoon. The results further show that the LSD plays a more fundamental role than topography in determining the extent of Asian and African monsoons, whereas the tropical zonal LSD and Asian mountains both play a crucial role for establishing summer monsoon convection over the South Asian region.

a. Influence of land–sea thermal contrast on the ASM

The influence of land–sea thermal contrast and plateau forcing on the ASM was also investigated by Wu et al. (2012c) through employing the GCM FGOALS_s. The model is integrated with prescribed, seasonally varying sea surface temperature (SST) and sea ice. The controlled climate integration is referred to as the CON experiment. Although the ASM intensity possesses a stronger bias compared with observation induced by stronger cross-equatorial flow, the modeled precipitation (Fig. 7-15a) in general captures the main features of the ASM compared with observations (Fig. 7-15b), performing reasonably well in simulating the maximum centers over the western coast of India, the Bay of Bengal, and the southeastern slopes of the TP.

Since the monsoon is traditionally considered an atmospheric response to the seasonal land–sea thermal contrast, it is reasonable to infer that the precipitation forced not by orography but by the land–sea distribution alone could be considered as a monsoon prototype. A no-mountain experiment NMT is thus designed, being the same as the CON run except that all the mountains worldwide are removed. The modeled precipitation

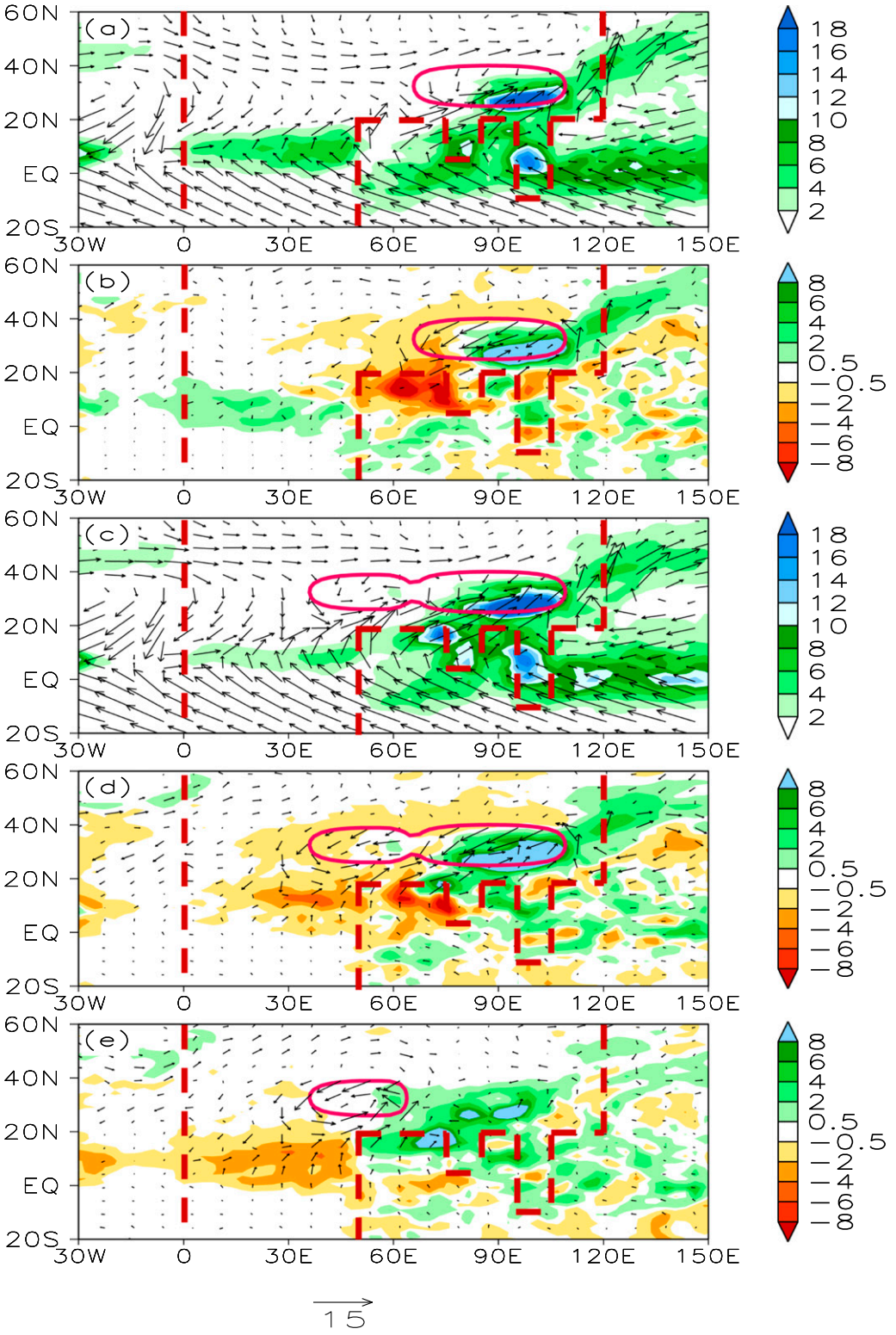

FIG. 7-13. Wind vectors at $\sigma = 0.991$ (arrows, m s^{-1}; the unit vector is shown at the bottom of the figure) and precipitation (shading; mm day^{-1}) in July (a) in Exp TP, and the difference between (b) Exp TP and Exp TRO; (c) in Exp IPTP, and (d) the difference between Exp IPTP and Exp TRO; and (e) the difference between Exp IPTP and Exp TP. The heavy red curve denotes the 700-m orographic contour; the heavy dashed line denotes the continent boundary [from Wu et al. (2012b)].

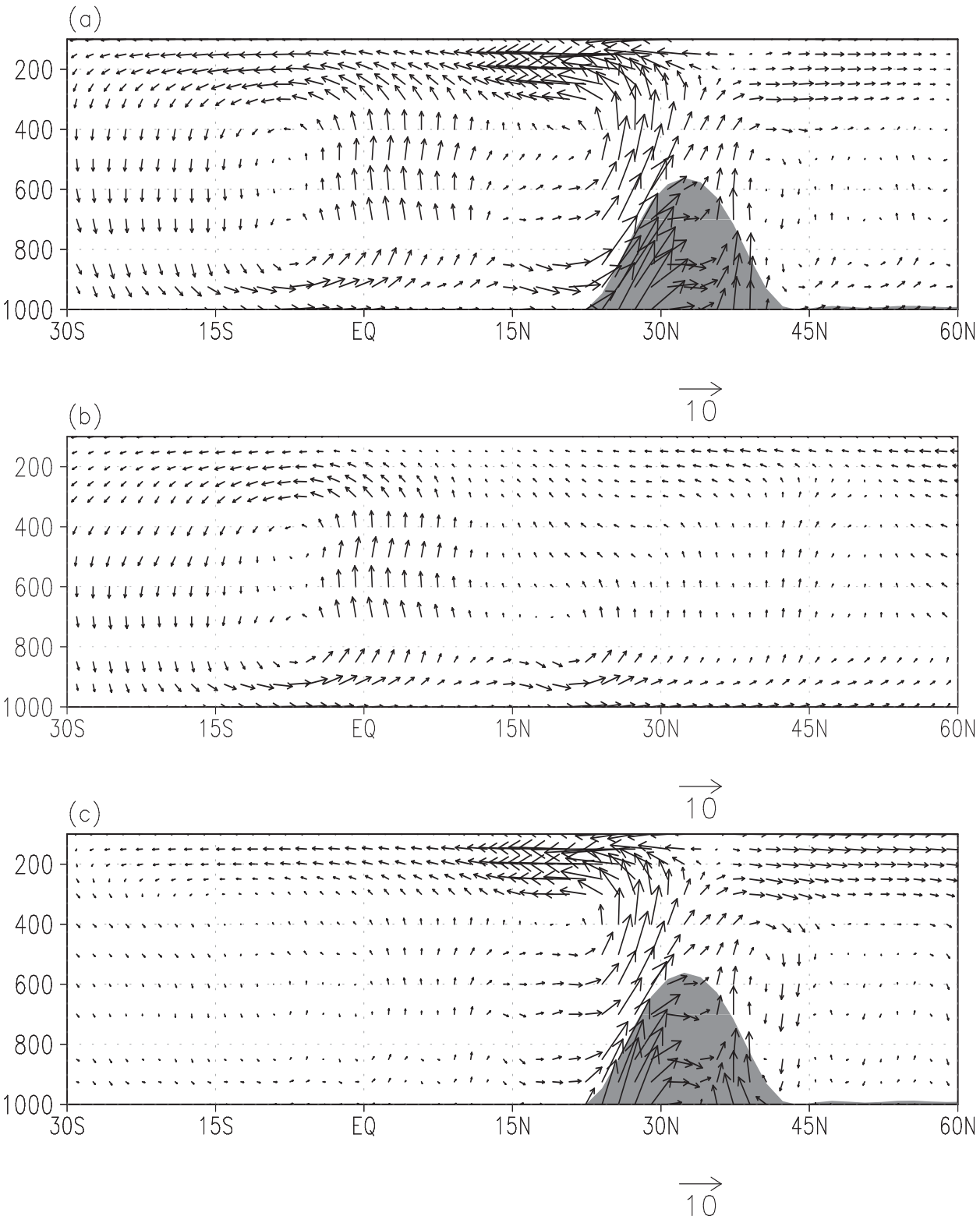

FIG. 7-14. Mean meridional circulation (v, $-\omega$; m s^{-1}) averaged over the eastern continent domain between 90° and 120°E in (a) Exp IPTP and (b) Exp TRO, and (c) their difference. The shading in (a),(c) denotes the TP shape across 87.5°E. The vertical pressure velocity ω has been amplified by -60 for better visibility [from Wu et al. (2012b)].

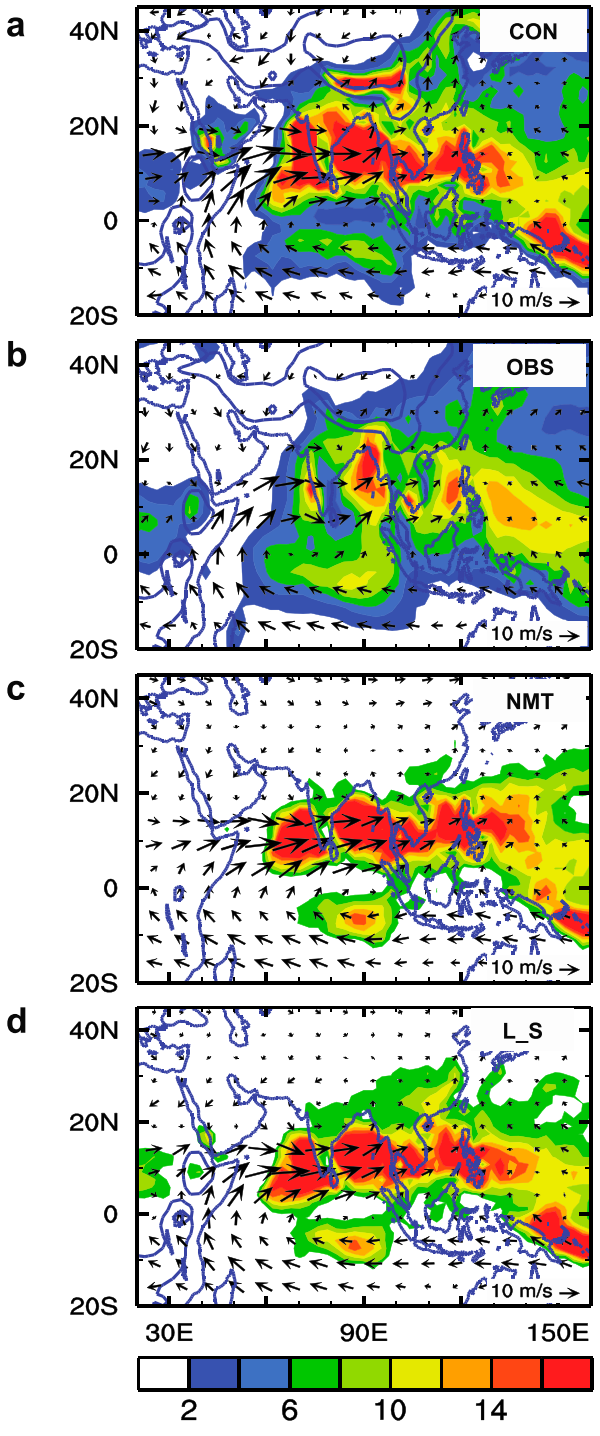

FIG. 7-15. Impacts of land–sea thermal contrast on the Asian summer monsoon showing the summer precipitation rate (color shading, mm day^{-1}) and 850-hPa winds (vectors, m s^{-1}) for (a) the control experiment CON; (b) observations averaged over the period 1979–2009 from Global Precipitation Climatology Project (GPCP) for precipitation and from NCEP–DOE AMIP-II Reanalysis (R-2) for winds; (c) experiment NMT in which the global surface elevations are set to zero; and (d) experiment L_S in which only the elevations of the Iranian Plateau (IP) and the Tibetan Plateau (TP) are set to zero. Contours in (a) and (b) over continental areas indicate elevations higher than 1500 and 3000 m [from Wu et al. (2012c)].

(Fig. 7-15c) is confined to south of 20°N, with the maximum centers (>18 mm day^{-1}) located between 10° and 15°N, as in the control run. Remarkable changes compared with the control run are seen in the subtropical area: the SASM north of 20°N and the East Asian summer monsoon (EASM) are substantially reduced. In an experiment in which only the IP and TP (Exp IPTP) is removed, the simulated precipitation pattern (Fig. 7-15d) is similar to that in NMT (Fig. 7-15c). Because our main concern is how the extensive Asian mountains IPTP influence the ASM, Fig. 7-15d could be considered a component of the ASM that is induced by land–sea thermal contrast alone. The experiment is thus termed the L_S experiment.

b. Influence of IPTP mechanical insulation on ASM

The differences (DIFF) in circulation and precipitation between CON (Fig. 7-15a) and L_S (Fig. 7-15d), as shown in Fig. 7-16a, are forced by mechanisms other than land–sea thermal forcing. Such mechanisms are required to 1) produce a cyclonic circulation at 850 hPa over the subtropical continent between 20° and 40°N, circumambulating the IPTP; 2) reduce precipitation over tropical oceans and the northwestern Pacific; and 3) increase precipitation mainly over the Asian continent, with maximum centers over India, the northern BOB, the southern slopes of the TP, and eastern Asia.

The absence of precipitation over northern India in the L_S experiment might reflect the removal of the ''IPTP insulator,'' which might result in the southward advection of dry, cold air from the subtropics and a lack of tropical convective instability and rainfall as proposed by Boos and Kuang (2010, hereinafter BK10). Were this the case, merely adding the IPTP (but not allowing its surface sensible heating to heat the atmosphere) into the L_S experiment, which is defined as the IPTP_M experiment, would be sufficient to produce the monsoon rainfall in the northern South Asia. However, the results in Fig. 7-16b indicate that this is not the case. In the IPTP_M experiment, the patterns of both precipitation and circulation at 850 hPa are similar to those in the L_S experiment. Similarly, if we merely add IP and TP separately into the L_S experiment (i.e., the IP_M and TP_M experiments, respectively), the resultant precipitation and circulation distributions (Figs. 7-16c and 7-16d, respectively) are also similar to those in the L_S experiment. These results demonstrate that in summer, mechanical insulation of the IP and TP has a minor influence on the generation of the ASM, as it cannot produce the required compensating rainfall and precipitation patterns as shown in Fig. 7-16a.

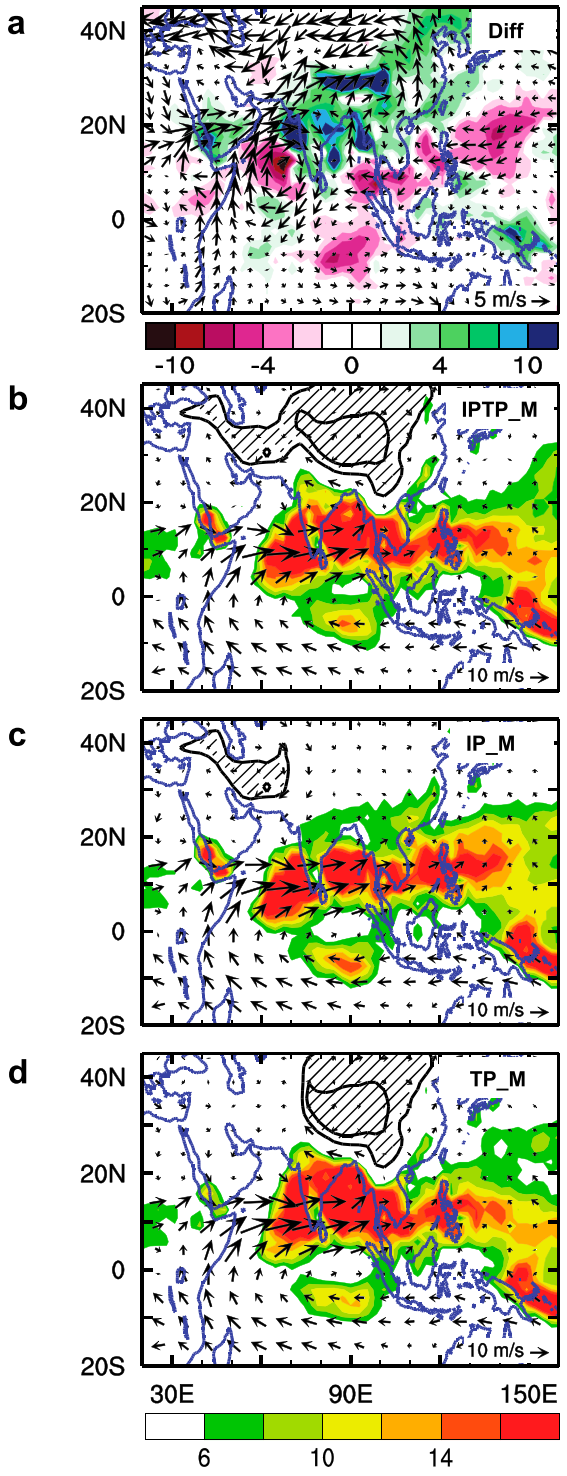

FIG. 7-16. As in Fig. 7-15 but for impacts of mountain mechanical forcing: (a) the difference (DIFF) between the CON and L_S experiments, indicating the compensating rainfall and circulation required to make up the total monsoon; (b) experiment IPTP_M in which the IP and TP mechanical forcing exists; (c) experiment IP_M in which the IP's mechanical forcing exists; and (d) experiment TP_M in which the TP's mechanical forcing exists. Thick black contours surrounding gray-hatched regions [except in (a)] indicate elevations higher than 1500 and 3000 m [from Wu et al. (2012c)].

c. Influence of IPTP thermal forcing on the ASM

Three sets of experiments were designed with surface sensible heating on the IP (IP_SH), TP (TP_SH), and IPTP (IPTP_SH), respectively, in order to study the influence of orographically elevated thermal forcing on the ASM. In IP_SH (Fig. 7-17a), the IP thermal forcing generates a cyclonic circulation encircling the IP, similar to the western parts of the compensating circulation in Fig. 7-16a. The forcing also results in reduced precipitation, mainly over the tropical Indian Ocean and the northwest Pacific, and increased precipitation over the Asian continent west of 100°E (especially over Pakistan, northern India, and the southwestern slopes of the TP), a pattern similar to that of the compensating precipitation west of 100°E, indicating the important role of the IP in generating the northern South Asian summer monsoon (SASM).

In the TP_SH experiment (Fig. 7-17b), TP thermal forcing also generates a cyclonic circulation encircling the TP. Correspondingly, reduced precipitation occurs west of 80°E; in contrast, increased precipitation occurs east of 80°E, especially over the BOB, the southern slopes of the TP, and East Asia. They are similar to the compensating precipitation and circulation patterns in the region east of 80°E (Fig. 7-16a), indicating that TP thermal forcing plays a dominant role in the generation of the EASM and the eastern part of the SASM.

In the IPTP_SH experiment (Fig. 7-17c), the elevated IPTP heating results in reduced precipitation in tropical oceans, and increased precipitation over the Asian continent to the north. The heating also generates a cyclonic circulation at 850 hPa over the Asian subtropical continental areas, with relatively isolated centers over the IP and TP. The results shown in Fig. 7-17c are basically equivalent to the linear addition of the results in Figs. 7-17a and 7-17b, indicating the important but contrasting roles of IP and TP thermal forcing in different parts of the ASM. More significantly, the precipitation and circulation patterns generated by IPTP thermal forcing (Fig. 7-17c) are close to those required to compensate the ASM (Fig. 7-16a). This result demonstrates that in addition to land–sea thermal contrast, the thermal forcing of large mountain ranges in Asia is an important factor in producing the ASM, especially over continental areas.

7. Topography-induced climbing and deflecting flow and configuration of ASM

a. Influence of climbing versus deflecting topographic effects on the ASM

More than 85% of the total atmospheric water vapor, as measured by specific humidity, generally resides in a layer below 3 km above sea level. In order for monsoon

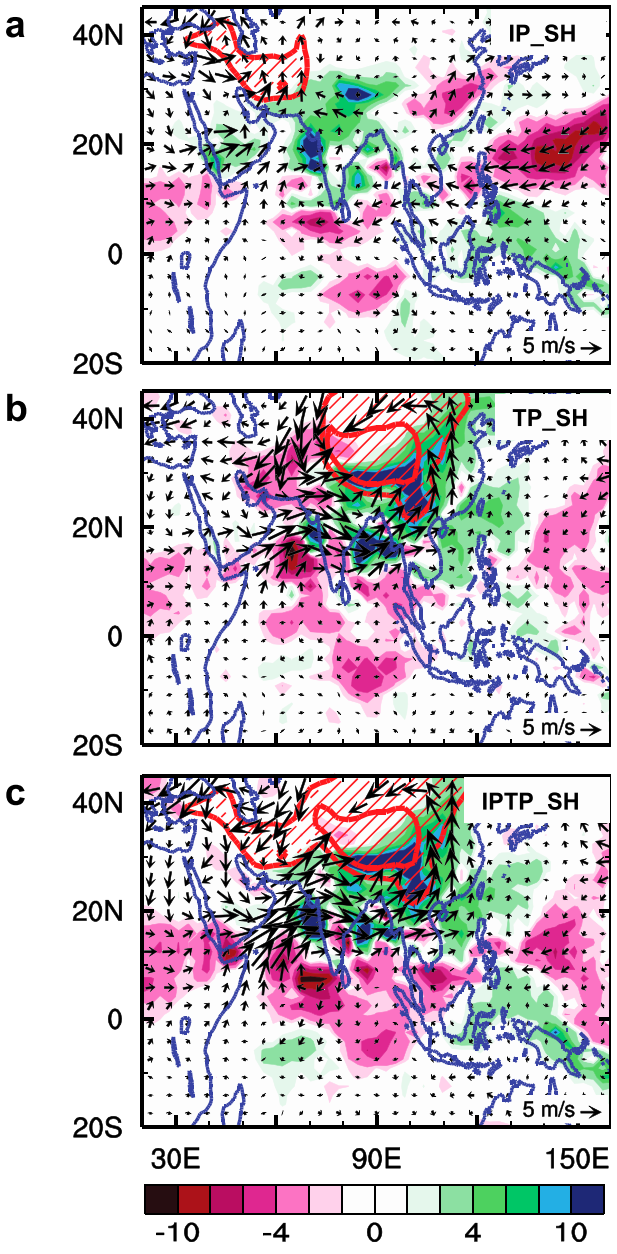

FIG. 7-17. As in Fig. 7-15, but for impacts of mountain thermal forcing generated by the elevated surface sensible heating of (a) the Iranian Plateau (IP_SH), (b) the Tibetan Plateau (TP_SH), and (c) the IP and TP (IPTP_SH). Thick red contours surrounding red-hatched regions indicate elevations higher than 1500 and 3000 m [from Wu et al. (2012c)].

clouds and precipitation to form, lower-tropospheric water vapor must be lifted by vertical motions forced either internally or externally. One of the internal forcings is the type of cold and/or warm fronts. This mechanism is important in middle and high latitudes, especially in winter, but is not important in the tropics in summer because the air temperature in the tropics is relatively uniform.

The mechanical forcing of mountains is an important external forcing: airflow impinging upon mountains is either deflected to produce encircling flow or lifted to produce climbing flow. Consequently, clouds and precipitation are generated around mountains. However, if a mountain is higher than several hundred meters, the conservation constraint of angular momentum and energy means that the airflow passes around the mountain rather than rising over it (Wu 1984).

Thermal forcing can also generate atmospheric ascent, because large-scale atmospheric potential temperature (θ) increases with height. According to the steady-state thermodynamic equation,

$$\mathbf{V} \cdot \nabla\theta = Q, \tag{7-1}$$

where $\mathbf{V}$ is air velocity. In regions of heating ($Q > 0$), air should penetrate isentropic surfaces upward. There are several types of atmospheric heating. Shortwave radiation is weakly absorbed directly by the atmosphere. In the absence of cloud, longwave radiation can easily escape into space. Condensation heating normally occurs above the cloud base. Surface sensible heating, however, can increase the near-surface entropy and result in the development of convective instability and trigger atmospheric ascent, and it is effective in generating atmospheric ascent in the lower troposphere.

If surface sensible heating occurs on a mountain slope, and if the mountain is high enough, large amounts of moisture in lower layers are readily transported to the free atmosphere. The TP in summer is a heat source for the atmosphere and has a strong influence on weather and climate. When a moist and warm southwesterly approaches the TP, the air becomes heated, starts to penetrate isentropic surfaces, and slides upward along its sloping surface.

Figure 7-18 shows the distribution of precipitation and streamlines at the $\sigma = 0.89$ surface, which is about 1 km from the surface. In the CON experiment (Fig. 7-18a), when the water conveyer belt originating from the Southern Hemisphere meanders eastward through the South Asian subcontinent, the effects of land–sea thermal forcing mean that severe precipitation centers are formed along 15°N. The rest of the water vapor is transported to sustain the East Asian monsoon, although some swerves northward over northern India and the BOB. The pumping effect of TP-SHAP results in the convergence of air toward the TP. The upward streamlines are perpendicular to the TP contours, eventually forming a cyclonic circulation at the southeastern corner of the TP. Consequently, heavy monsoon rainfall occurs over northern India and western China, with a maximum center ($>18\,\text{mm day}^{-1}$) appearing over the

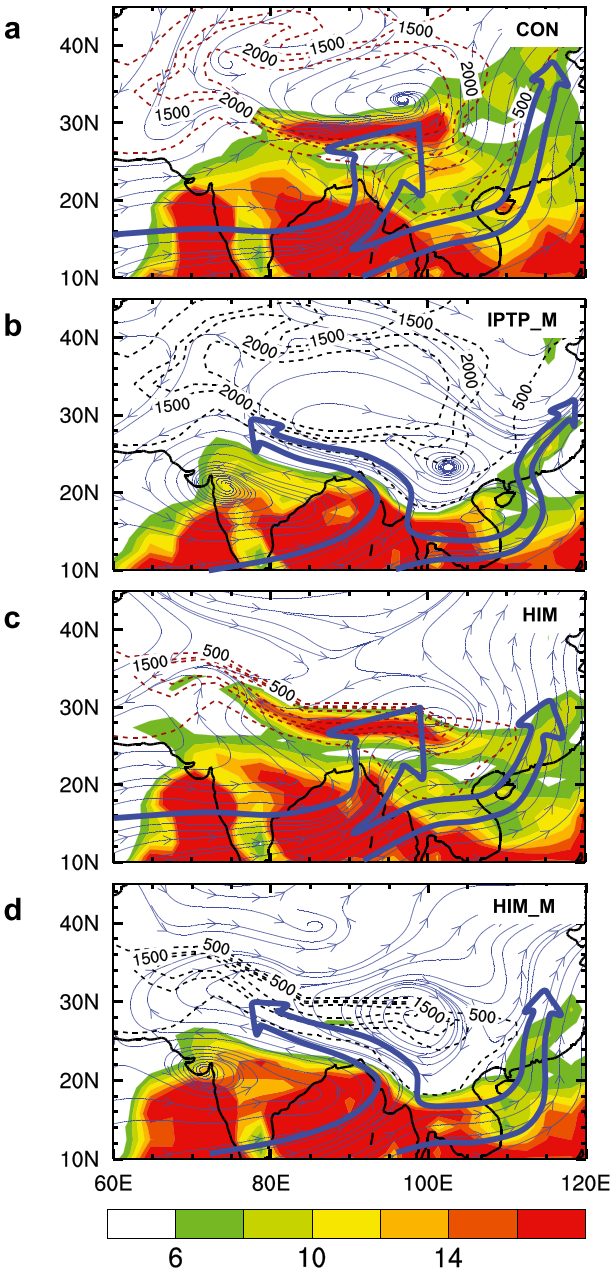

FIG. 7-18. Mechanisms and relative contributions of the climbing and deflecting effects of mountains, showing the summer precipitation rate (color shading, mm day^{-1}) and streamlines at the σ = 0.89 level for the (a) CON, (b) IPTP_M, (c) HIM, and (d) HIM_M experiments. Dashed contours enclose elevations higher than 1500 and 3000 m with red and black colors, respectively, indicating with and without surface sensible heating of the mountains. Dark blue open arrows denote the main atmospheric flows impinging on the TP, either climbing up the plateau in (a) and (c) or moving around the plateau, parallel to orographic contours, in (b) and (d). [Adapted from Wu et al. (2012c).]

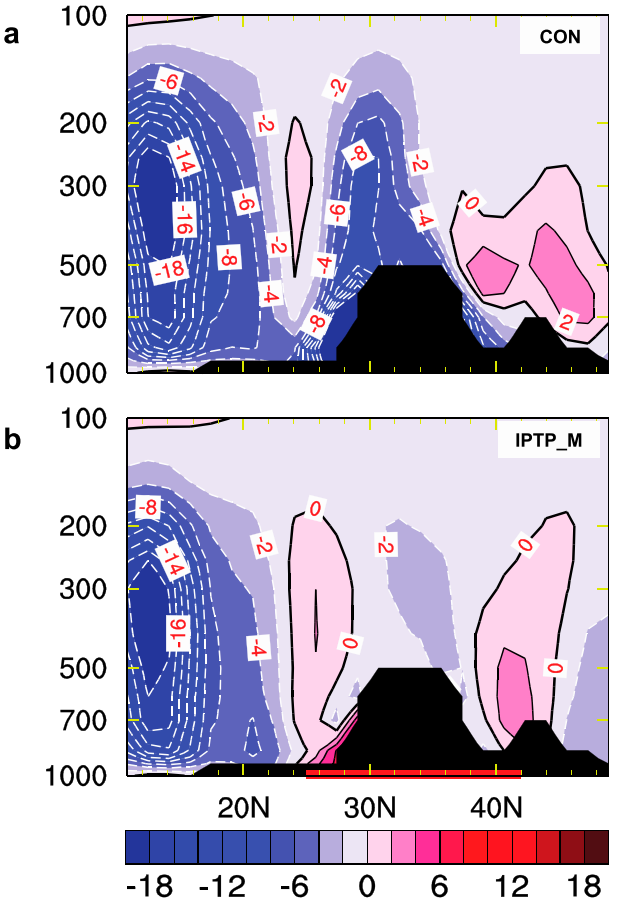

FIG. 7-19. Structure of the South Asian summer monsoon, showing 80°–90°E longitudinally averaged vertical–meridional cross sections of pressure vertical velocity (contour interval, 2 × 10^{-2} Pa s^{-1}) for experiments (a) CON and (b) IPTP_M. The black mass indicates the topography [from Wu et al. (2012c)].

southeastern slopes of the TP. The condensation heating of this rainfall center generates cyclonic circulation in the lower layer and further intensifies the EASM.

In the IPTP_M experiment (Fig. 7-18b), in contrast, when the water vapor flux from the main water conveyer belt approaches the TP, it is not heated and the airflow remains at the same isentropic surface [Eq. (7-1)]. Consequently, the streamlines do not climb up the TP; instead, they move around the mountains, parallel to orographic contours. Thus, no monsoon develops over northern India and the TP, and the EASM is substantially weakened. These results indicate that the thermal forcing of large-scale mountains plays a dominant role in the generation of the northern and eastern parts of the SASM and the EASM.

Boos and Kuang claimed that the impact of TP thermal forcing is less important than the thermal insulation of the Himalayas in the formation of the SASM (BK10;

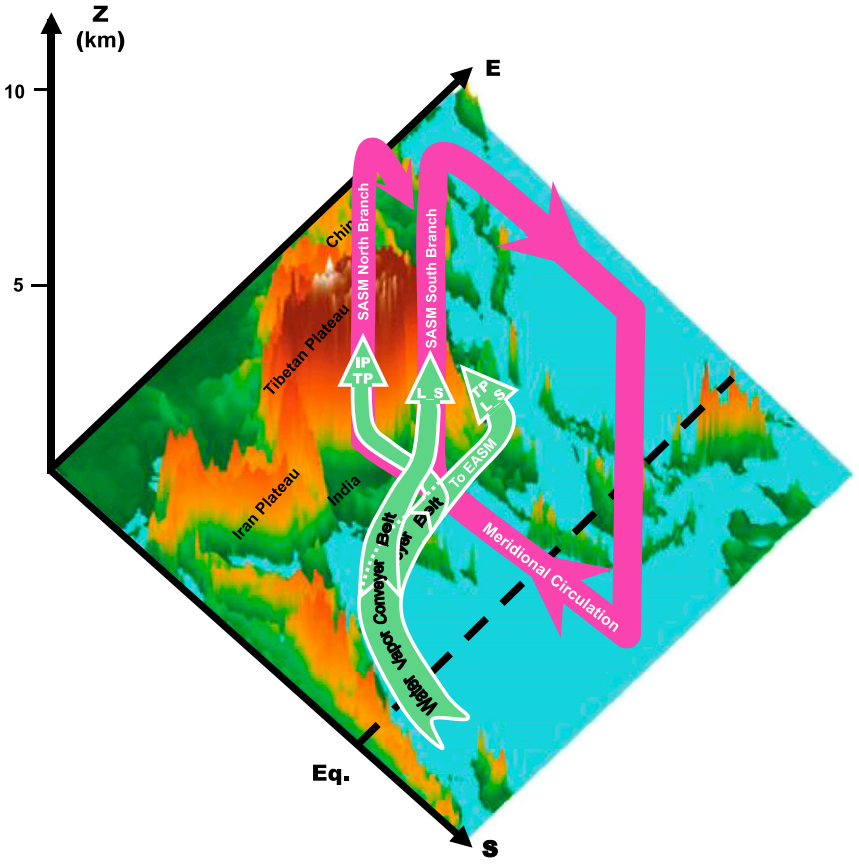

FIG. 7-20. Schematic diagram showing the gross structure of the Asian summer monsoon. For the southern branch, water vapor along the conveyer belt is lifted up due mainly to land–sea (L_S) thermal contrast in the tropics; for the northern branch, the water vapor is drawn away from the conveyer belt northward toward the foothills and slopes of the TP, and is uplifted to produce heavy precipitation that is controlled mainly by IPTP-SHAP; the rest of the water vapor is transported northeastward to sustain the East Asian summer monsoon, which is controlled by the land–sea thermal contrast as well as thermal forcing of the TP [adapted from Wu et al. (2012c)].

Boos and Kuang 2013). Their conclusion was based on a numerical experiment in which the main part of TP was removed while only its southern rim (the Himalayas) is maintained and the resultant SASM was similar to that in the control experiment with the whole TP presented. They proposed that the Himalayas block cold, dry air from the north and the high surface entropy over India can thus induce moist convection and drive the SASM. Wu et al. (2012c) followed BK10's experiment design based on the FGOALS model and carried a similar numerical experiment (HIM). The modeled SASM rainfall as shown in Fig. 7-18c is also similar to that in the CON run (Fig. 7-18a) as reported by BK10. However, in a parallel experiment HIM_M, which is the same as HIM but without surface sensible heating from the Himalaya to the atmosphere, the northern branch of the SASM disappeared completely (Fig. 7-18d) as in the IPTP_M run (Fig. 7-18b). Since in the HIM_M experiment the insulation effect is kept as in HIM, the results demonstrate that the insulation effect of the TP is insignificant in the formation of the SASM and the thermal pumping of the IPTP plays a fundamental role. Notice that in all the numerical experiments in which topography is removed (e.g., Kasahara and Washington 1971; Hahn and Manabe 1975; BK10), there was no cold and dry advection in summer from the subtropics to northern India. This is because in summer the subtropical area is warmer than in the tropics. Furthermore, the high surface entropy over northern India depends on high surface temperature as well as high humidity. It is due to the pumping effect of the IPTP that the abandoned moisture over ocean can be transported into inland India and result in high surface entropy there. In this regard the SASM is also thermally controlled.

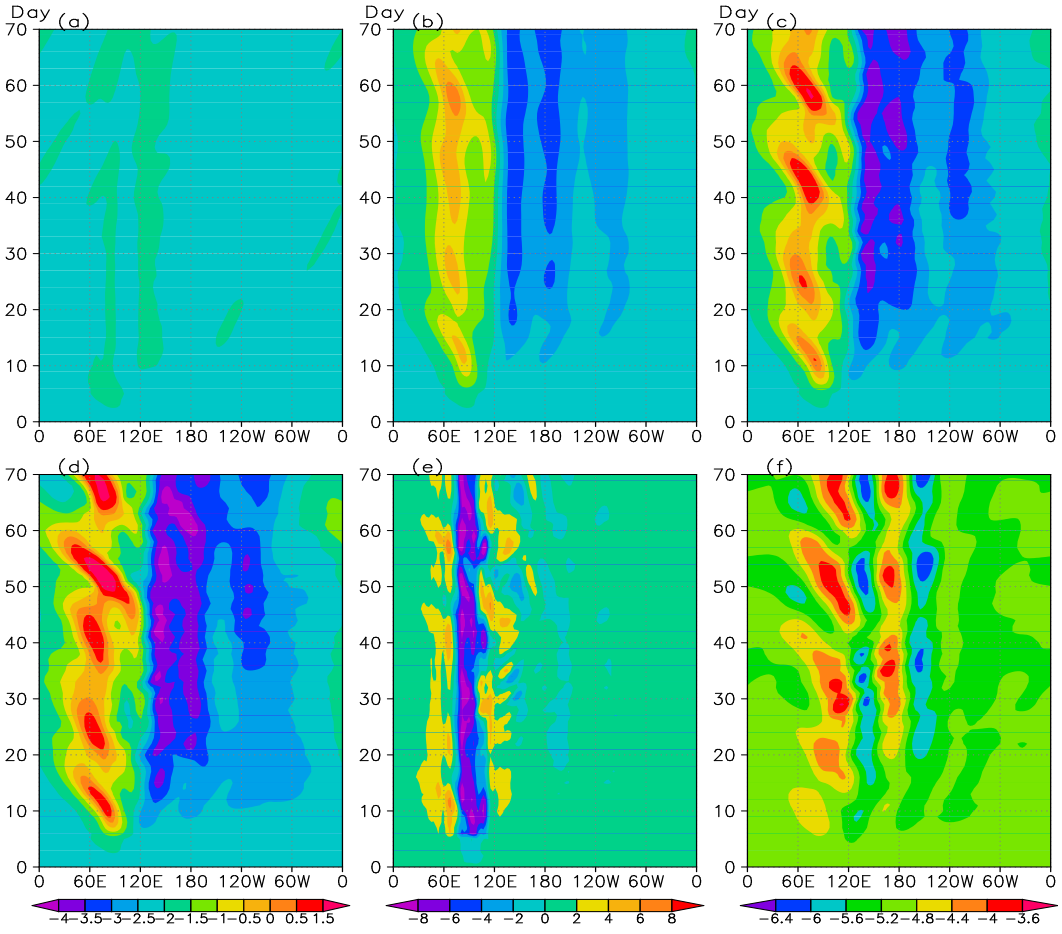

FIG. 7-21. Time–longitude cross section of 25°–35°N averaged 200-hPa streamfunction ($10^7\,m^2\,s^{-1}$) for (a) the O_TP experiment (simulation only with the TP orography), (b) the OQ_TP experiment (with the TP orography and observed heating above), (c) the O1.6Q_TP experiment (with the TP orography and 1.6 times heating above), and (d) the O2Q_TP experiment (with the TP orography and 2 times heating above). Panels (e),(f) are similar to (a) but for ω at 400 hPa (10^{-2} Pa s^{-1}) and for the 40°–60°N averaged 250-hPa streamfunction in the O1.6Q_TP experiment, respectively. The left color bar underneath the panels is for the streamfunction in (a)–(d), the middle bar for ω, and the right bar for the streamfunction in (f) [from Liu et al. (2007b)].

b. Structure of the ASM

A striking feature of the above experiments is the insensitivity of the southern part of the SASM to IPTP forcing: actually in all experiments (Figs. 7-15, 7-16, and 7-18), the intensity and spatial distribution of precipitation south of 20°N show little change compared with the control while the configuration or thermal status of the Tibetan/Iranian Plateau shows a marked change. Figures 7-19a and 7-19b show 80°–90°E longitudinally averaged latitude–height cross sections from the CON and IPTP_M experiments, demonstrating that the vertical velocity is divided into a southern branch near 15°N and a northern branch at about 25°N. In the CON run (Fig. 7-19a), strong rising associated with the southern SASM is located over the northern Indian Ocean. Ascending air is also dominant above the TP, with maxima located near the surface, indicating the importance of surface sensible heating in generating orographic ascent. In the IPTP_M experiment (Fig. 7-19b), the lack of surface heating on the TP results in two remarkable sinking centers over its slopes; thus, the northern branch of the SASM disappears over northern India. However, the intensity and location of the southern branch is largely unchanged. In fact, in all the experiments the southern SASM branch remains steady, with a center ($>18\times10^{-2}$ Pa s^{-1}) at about 400 hPa, locked to the south of the coastline. The insensitivity of the southern branch of the SASM to orographic change indicates that the land–sea thermal contrast plays a dominant role in its generation and variation.

The above discussion is summarized schematically in Fig. 7-20. The meridional circulation of the SASM can

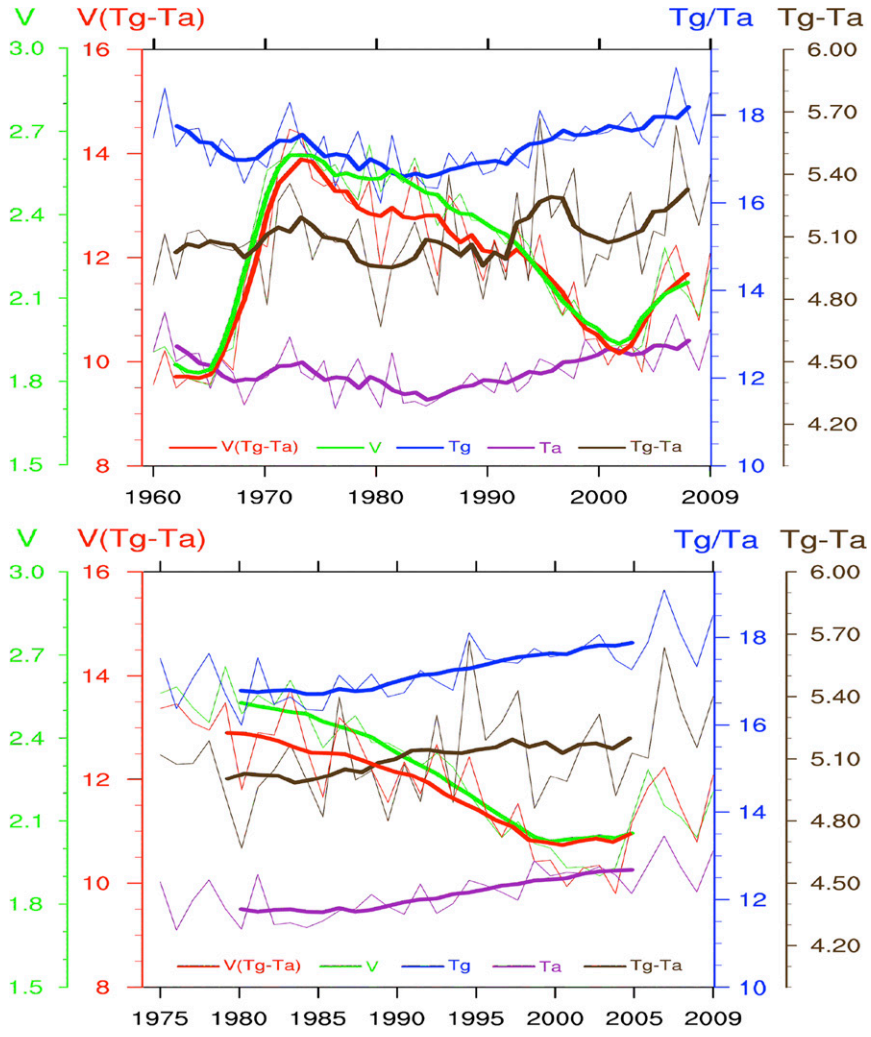

FIG. 7-22. Evolutions of JJA means averaged over the Tibetan Plateau stations of surface soil temperature T_g, surface air temperature T_a, difference between T_g and T_a, surface wind speed V, and the parameter of surface sensible heat flux PSH $= V(T_g - T_a)$. Values shown are (a) for 1960–2009 and for the corresponding 5-yr running mean and (b) for 1975–2009 and the corresponding 11-yr running mean. Units are °C for T_g, T_a, and $(T_g - T_a)$; m s^{-1} for V; and °C m^{-1} s^{-1} for PSH [from Liu et al. (2012)].

be divided into southern and northern branches. Its southern branch is located in the tropics: water vapor that originates from the Southern Hemisphere and is transported along the zonally oriented "water vapor conveyer belt" is lifted upward due to the land–sea thermal contrast, forming monsoon precipitation there. The northern branch occurs along the southern margin of the IPTP in the subtropics. When the conveyer belt approaches the TP, part of its water vapor is hauled away and turned northward, then lifted upward by the IPTP-SHAP, resulting in heavy precipitation in the monsoon trough over northern India and along the foothills and slopes of the TP. The rest of the water vapor along the water conveyer belt is transported northeastward to sustain the EASM, which is controlled by the land–sea thermal contrast and thermal forcing of the TP. These results highlight the dominant roles of the land–sea thermal contrast and IPTP thermal forcing in influencing the ASM.

8. Variation of the thermal forcing over the TP and its impacts

The real atmosphere goes through periods in which the monsoon variability is suppressed or enhanced depending on the intensities of the TP and tropical heating and the vertical extent of the heating in the TP region.

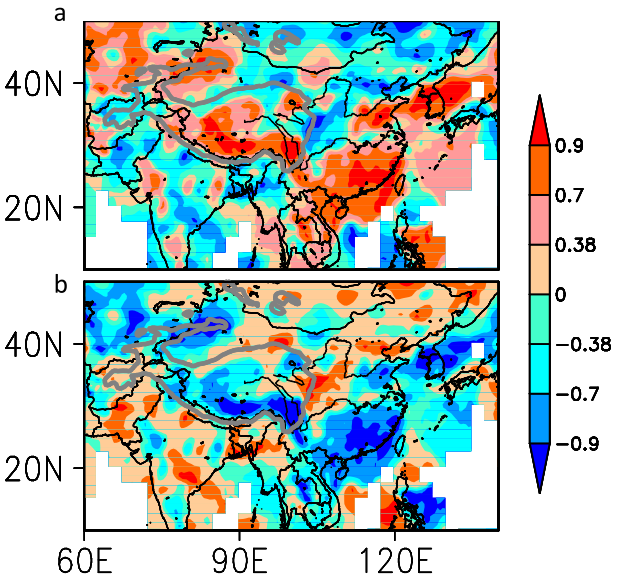

FIG. 7-23. Distributions of the correlation coefficient for 1980–2004 and between the June–August (JJA) precipitation and the TP-averaged (a) T_a and (b) PSH = V (T_g − T_a). The source data were processed using 11-yr running mean before the correlation calculation was performed. The heavy gray contours are the main body of the TP [adapted from Liu et al. (2012)].

a. Biweekly oscillation of the South Asian anticyclone

Severe weather events in China and in the Asian monsoon regions have been found to have a close relationship with the nature of the Tibetan upper tropospheric anticyclone, the South Asian anticyclone (SAA). A quasi-periodic oscillation of the SAA was revealed in the spectral analysis performed by Tao and Zhu (1964) and Tao and Ding (1981) with periods of 10–16 days. Liu et al. (2007b) found that heating over the plateau leads to a potential vorticity (PV) minimum and that if it is sufficiently strong, say 1.5 or 2 times the observed average, the flow is unstable, producing a quasi-biweekly oscillation (Figs. 7-21c,d). During this oscillation, the Tibetan anticyclone changes from a single center over the southwestern side of the plateau to a split–double structure with centers over China and the Middle East and back again. These characteristics are similar to observed variability in the region. Associated with this quasi-biweekly oscillation are significant variations in the strength of the ascent over the plateau (Fig. 7-21e) and the Rossby wave pattern over the North Pacific (Fig. 7-21f).

The origin of the variability is instability associated with the zonally extended potential vorticity PV minimum on a θ surface, as proposed by Hsu and Plumb (2000). This minimum is due to the tendency to reduce the PV above the heating over the plateau and to advection by the consequent anticyclone of high PV around from the east and low PV to the west. The deep convection to the south and southeast of the plateau tends to suppress the quasi-biweekly oscillation because the low PV produced above it acts to reduce the meridional PV gradient reversal. The occurrence of the oscillation depends on the relative magnitude of the heating in the two regions (Liu et al. 2007a,b).

b. Decadal variation of the TP thermal forcing and the rainfall in East China

Duan et al. (2006) and Duan and Wu (2008) reported that temporal change in the annual-mean surface atmospheric temperature T_a over the plateau increased at a rate of 0.4°C decade^{-1} during the period of 1980–2003. Data analysis based on station observations reveals that many meteorological variables averaged over the TP are closely correlated, and their trends during the past decades are well correlated with the rainfall trend of the Asian summer monsoon. Liu et al. (2012) and Zhu et al. (2012) further diagnosed and confirmed the existence of a weakening decadal trend in TP thermal forcing from the mid-1970s to the end of the 1990s, characterized by weakened surface sensible heat flux in spring and summer (Fig. 7-22). They also indicated that the weakening trend in surface sensible heating is highly correlated with surface wind speed V. This weakening trend in thermal forcing is significantly correlated with decreasing summer precipitation over northern South Asia and northern China and increasing precipitation over northwestern China, southern China, and the Korean peninsula during the same period (Fig. 7-23).

However, such a correlation does not necessarily imply causality. An atmospheric general circulation model, the HadAM3, was employed to elucidate the causality between the weakening TP forcing (Fig. 7-24) and the change in the Asian summer monsoon rainfall. Results demonstrate that a weakening in surface sensible heating over the TP results in reduced summer precipitation in the plateau region and a reduction in the associated latent heat release in summer (Fig. 7-24a). These changes in turn result in the weakening of the near-surface cyclonic circulation surrounding the plateau and the subtropical anticyclone over the subtropical western North Pacific (Fig. 7-24b), in agreement with the results obtained from the idealized TP experiment (Fig. 7-13b) but with opposite polarities. The southerly that normally dominates East Asia, ranging from the South China Sea to northern China, then weakens, resulting in a weaker equilibrated Sverdrup balance between positive vorticity generation and latent heat release. Consequently, the convergence of water vapor transport is confined to southern China, forming a unique anomaly pattern in monsoon rainfall (Fig. 7-24c), "south wet and north dry."

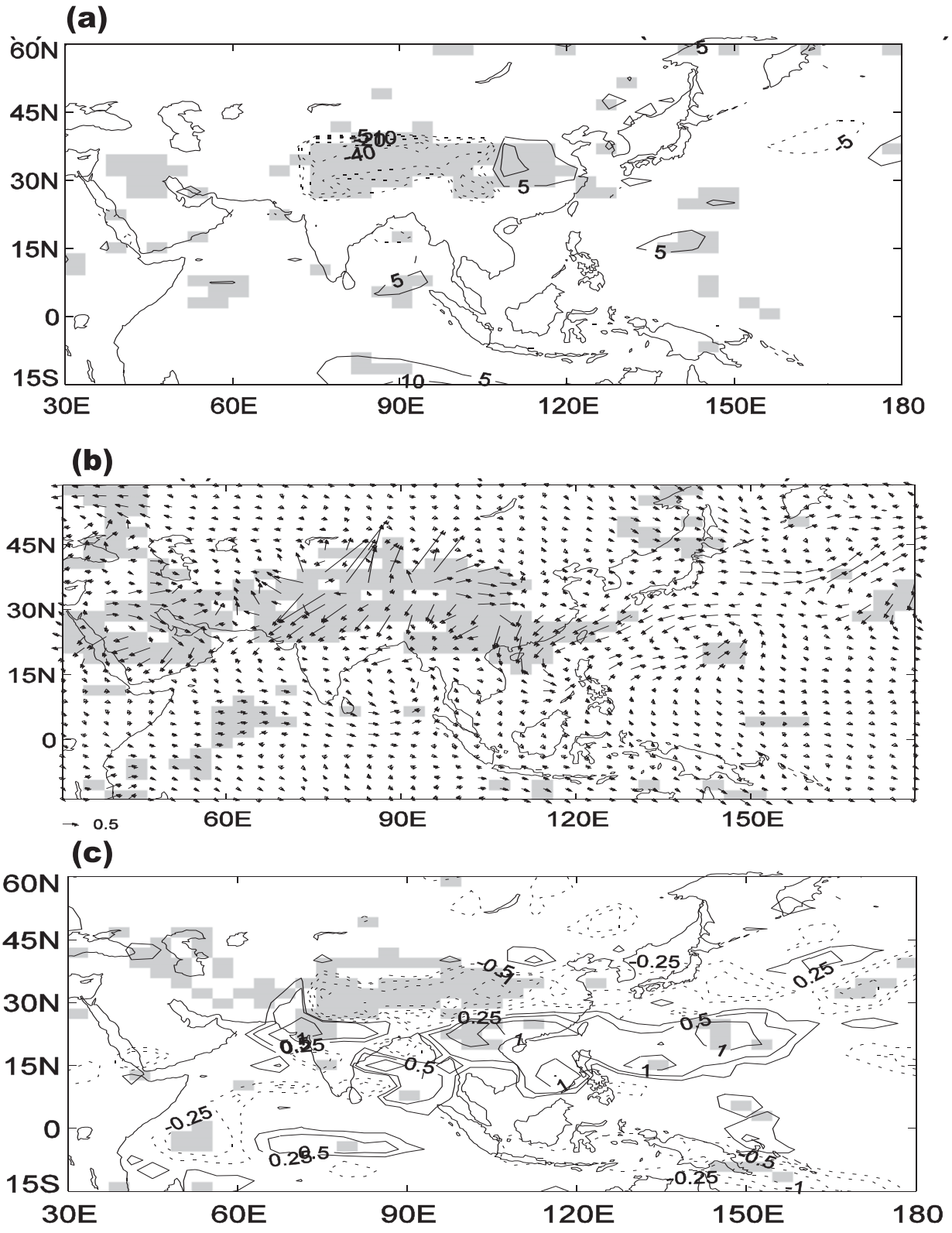

FIG. 7-24. Weakening TP thermal forcing: monthly difference between experiment albedo increase (Exp Albedo-I) and experiment albedo decrease (Exp Albedo-D) in terms of the JJA-mean (a) surface upward sensible and latent heat flux anomalies ($W\,m^{-2}$), (b) surface wind ($m\,s^{-1}$), and (c) precipitation ($mm\,day^{-1}$). Shading indicates regions where anomalies are significant at the 95% confidence level (*t* test) [adapted from Liu et al. (2012)].

It is interesting to see that the summertime surface sensible heating over the TP has strengthened since the beginning of this century (Fig. 7-22). A similar result was also found by Si and Ding (2013) based on the 72 stations over the central and eastern TP. This then implies that the wet south and dry north rainfall anomaly pattern over eastern China may come to an end and an opposite pattern may appear in the near future.

9. Future perspective

In nature, the influences of the IPTP orography and its surface sensible heating cannot be separated. The significance of the dominance of IPTP thermal forcing in influencing the ASM lies in the fact that, over the modern-day orography, the thermal status of the IPTP varies due to natural and anthropogenic factors. By focusing on changes in the thermal status of the IPTP, the dominance of thermal controls on the ASM may provide us with a tangible way of identifying climate trends in the Asian summer monsoon in a warming world, and of improving weather forecasts, climate predictions, and projections in areas affected by the Asian monsoon. The challenges could be to 1) understand the modulation of the TP on the air–sea interaction and 2) quantify the impact of the TP.

The modulation of the TP on air–sea interaction is a newly recognized monsoon dynamic. How such modulation influences the seasonal and interannual variability of the ASM and the ENSO–monsoon relationship must be further studied.

Quantifying the TP impact is crucial for the further understanding and predictions of the Asian monsoon. It is necessary to increase in situ observation stations, improve the quality of the satellite data over the plateau, improve the description of physical processes in numerical models—boundary processes, cloud, radiation, convection, etc.,—over the plateau. Work will focus on identifying and explaining potentially significant teleconnections, such as the influence of Tibetan snow cover on the Asian monsoon and Northern Hemispheric conditions. Employing existing theories in physics, chemistry, and mathematics to reveal the complex and relevant multisphere interaction and to get new insights into the impacts of the TP on climate will be significant for enhancing our understanding the roles of the TP in regional and global climate and improving the fidelity of climate model and prediction.

Acknowledgments. Material used here is based on cooperative studies among the authors and Drs. Buwen Dong, Anmin Duan, Qiong Zhang, Weiping Li, Xin Liu, Xiaoyun Liang, Tongmei Wang, Zaizhi Wang, JingjingYu, Jieli Hong, and Yue Guan.

REFERENCES

Bao, Q., G. Wu, Y. Liu, Y. Jing, Z. Wang, and T. Zhou, 2010: An introduction to the coupled model FGOALS1.1-s and its performance in East Asia. *Adv. Atmos. Sci.*, **27**, 1131–1142, doi:10.1007/s00376-010-9177-1.

Boos, W. R., and Z. Kuang, 2010: Dominant control of the South Asian monsoon by orographic insulation versus plateau heating. *Nature*, **463**, 218–222, doi:10.1038/nature08707.

——, and ——, 2013: Sensitivity of the South Asian monsoon to elevated and non-elevated heating. *Sci. Rep.*, **3**, 1192, doi:10.1038/srep01192.

Chang, C.-P., Ed., 2004: *East Asian Monsoon*. World Scientific, 564 pp.

——, Z. Wang, and H. Hendon, 2006: The Asian winter monsoon. *The Asian Monsoon*, B. Wang et al., Eds., Springer, 89–127.

Charney, J. G., and P. G. Drazin, 1961: Propagation of planetary-scale disturbances from the lower into the upper atmosphere. *J. Geophys. Res.*, **66**, 83–109, doi:10.1029/JZ066i001p00083.

Chen, P., 2001: Thermally forced stationary waves in a quasigeostrophic system. *J. Atmos. Sci.*, **58**, 1585–1594, doi:10.1175/1520-0469(2001)058<1585:TFSWIA>2.0.CO;2.

Duan, A. M., and G. X. Wu, 2005: Role of the Tibetan Plateau thermal forcing in the summer climate patterns over subtropical Asia. *Climate Dyn.*, **24**, 793–807, doi:10.1007/s00382-004-0488-8.

——, and ——, 2008: Weakening trend in the atmospheric heat source over the Tibetan Plateau during recent decades. Part I: Observations. *J. Climate*, **21**, 3149–3164, doi:10.1175/2007JCLI1912.1.

——, ——, Q. Zhang, and Y. Liu, 2006: New proofs of the recent climate warming over the Tibetan Plateau as a result of the increasing greenhouse gases emissions. *Chin. Sci. Bull.*, **51**, 1396–1400, doi:10.1007/s11434-006-1396-6.

Flohn, H., 1957: Large-scale aspects of the ''summer monsoon'' in South and East Asia. *J. Meteor. Soc. Japan*, 75th anniversary volume, 180–186.

Hahn, D. G., and S. Manabe, 1975: The role of mountains in the South Asian monsoon circulation. *J. Atmos. Sci.*, **32**, 1515–1541, doi:10.1175/1520-0469(1975)032<1515:TROMIT>2.0.CO;2.

Held, I. M., 1983: Stationary and quasi-stationary eddies in the extratropical troposphere: Theory. *Large-Scale Dynamical Processes in the Atmosphere*, B. Hoskins and R. Pearse, Eds., Academic Press, 127–168.

Holton, J. R., 2004: *An Introduction to Dynamic Meteorology*. Elsevier Academic, 535 pp.

Hsu, C. J., and R. A. Plumb, 2000: Nonaxisymmetric thermally driven circulations and upper-tropospheric monsoon dynamics. *J. Atmos. Sci.*, **57**, 1255–1276, doi:10.1175/1520-0469(2000)057<1255:NTDCAU>2.0.CO;2.

Kasahara, A., and W. M. Washington, 1971: General circulation experiments with a six-layer NCAR model, including orography, cloudiness, and surface temperature calculations. *J. Atmos. Sci.*, **28**, 657–701, doi:10.1175/1520-0469(1971)028<0657:GCEWAS>2.0.CO;2.

Krishnamurti, T. N., 1981: Cooling of the Arabian Sea and the onset-vortex during 1979. Recent progress in equatorial oceanography: A report of the final meeting of SCOR Working Group 47, Scientific Committee on Oceanic Research, 1–12.

Li, L. F., Y. M. Liu, and C. Y. Bo, 2011: Impacts of diabatic heating anomalies on an extreme snow event over South China in January 2008 (in Chinese). *Climatic Environ. Res.*, **16**, 126–136.

Liang, X. Y., Y. M. Liu, and G. X. Wu, 2005: Effect of Tibetan Plateau on the site of onset and intensity of the Asian summer monsoon (in Chinese). *Acta Meteor. Sin.*, **63**, 799–805.

Liu, X., G. X. Wu, W. P. Li, and Y. M. Liu, 2001: Thermal adaptation of the large-scale circulation to the summer heating over the Tibetan Plateau (in Chinese). *Prog. Nat. Sci.*, **11**, 207–214.

——, W. P. Li, and G. X. Wu, 2002: Interannual variations of the diabatic heating over the Tibetan Plateau and the Northern Hemispheric circulation in summer. *Acta Meteor. Sin.*, **60**, 267–277.

Liu, Y. M., G. X. Wu, H. Liu, and P. Liu, 2001: Condensation heating of the Asian summer monsoon and the subtropical anticyclone in the Eastern Hemisphere. *Climate Dyn.*, **17**, 327–338, doi:10.1007/s003820000117.

——, J. C. L. Chan, J. Y. Mao, and G. X. Wu, 2002: The role of Bay of Bengal convection in the onset of the 1998 South China Sea summer monsoon. *Mon. Wea. Rev.*, **130**, 2731–2744, doi:10.1175/1520-0493(2002)130<2731:TROBOB>2.0.CO;2.

——, Q. Bao, A. M. Duan, Z. A. Qian, and G. X. Wu, 2007a: Recent progress in the study in China of the impact of Tibetan Plateau on the climate. *Adv. Atmos. Sci.*, **24**, 1060–1076, doi:10.1007/s00376-007-1060-3.

——, B. J. Hoskins, and M. Blackburn, 2007b: Impact of Tibetan topography and heating on the summer flow over Asia. *J. Meteor. Soc. Japan*, **85B**, 1–19, doi:10.2151/jmsj.85B.1.

——, G. X. Wu, J. L. Hong, B. Dong, A. Duan, Q. Bao, and L. J. Zhou, 2012: Revisiting Asian monsoon formation and change associated with Tibetan Plateau forcing: II. Change. *Climate Dyn.*, **39**, 1183–1195, doi:10.1007/s00382-012-1335-y.

Mao, J. Y., and A. M. Duan, 2005: The predictability of the reversal of the ridge of the subtropical anticyclone and the onset of the summer Asian monsoon (in Chinese). *Impacts of the Land–Sea Thermal Contrast on the Climate in China*, Y. Liu and Z. Qian, Eds., China Meteorological Press, 173–177.

——, G. Wu, and Y. Liu, 2002a: Study on modal variation of subtropical high and its mechanism during seasonal transition. Part I: Climatological features of subtropical high structure (in Chinese). *Acta Meteor. Sin.*, **60**, 400–408.

——, ——, and ——, 2002b: Study on modal variation of subtropical high and its mechanism during seasonal transition. Part II: Seasonal transition index over Asian monsoon region (in Chinese). *Acta Meteor. Sin.*, **60**, 409–420.

Nigam, S., 1994: On the dynamical basis for the Asian summer monsoon rainfall–El Niño relationship. *J. Climate*, **7**, 1750–1771, doi:10.1175/1520-0442(1994)007<1750:OTDBFT>2.0.CO;2.

——, 1997: The annual warm to cold phase transition in the eastern equatorial Pacific: Diagnosis of the role of stratus cloud-top cooling. *J. Climate*, **10**, 2447–2467, doi:10.1175/1520-0442(1997)010<2447:TAWTCP>2.0.CO;2.

Si, D., and Y.-H. Ding, 2013: Decadal change in the correlation pattern between the Tibetan Plateau winter snow and the East Asian summer precipitation during 1979–2011. *J. Climate*, **26**, 7622–7634, doi:10.1175/JCLI-D-12-00587.1.

Tao, S.-Y., and F. K. Zhu, 1964: The variation of 100-mb circulation over South Asia in summer and its association with march and withdrawal of the West Pacific subtropical high (in Chinese). *Acta Meteor Sin.*, **34**, 385–395.

——, and Y.-H. Ding, 1981: Observational evidence of the influence of the Qinghai-Xizang (Tibet) Plateau on the occurrence of heavy rain and severe convective storms in China. *Bull. Amer. Meteor. Soc.*, **62**, 23–30, doi:10.1175/1520-0477(1981)062<0023:OEOTIO>2.0.CO;2.

——, and L. Chen, 1987: A review of recent research on the East Asian summer monsoon in China. *Monsoon Meteorology*, Oxford University Press, 60–92.

Tian, S. F., and T. Yasunari, 1998: Climatological aspects and mechanism of spring persistent rains over central China. *J. Meteor. Soc. Japan*, **76**, 57–71.

Wallace, J. M., and P. V. Hobbs, 1977: *Atmospheric Science: An Introductory Survey*. Academic Press, 467 pp.

Wan, R. J., and G. X. Wu, 2007: Mechanism of the spring persistent rains over southeastern China. *Sci. China*, **50D**, 130–144, doi:10.1007/s11430-007-2069-2.

Wang, B., 2006: *The Asian Monsoon*. Springer, 787 pp.

——, and LinHo, 2002: Rainy seasons of the Asian-Pacific monsoon. *J. Climate*, **15**, 386–398, doi:10.1175/1520-0442(2002)015<0386:RSOTAP>2.0.CO;2.

Wu, G. X., 1984: The nonlinear response of the atmosphere to large-scale mechanical and thermal forcing. *J. Atmos. Sci.*, **41**, 2456–2476, doi:10.1175/1520-0469(1984)041<2456:TNROTA>2.0.CO;2.

——, and Y. S. Zhang, 1998: Tibetan Plateau forcing and the timing of the monsoon onset over South Asia and the South China Sea. *Mon. Wea. Rev.*, **126**, 913–927, doi:10.1175/1520-0493(1998)126<0913:TPFATT>2.0.CO;2.

——, W. Li, H. Guo, H. Liu, J. Xue, and Z. Wang, 1997: Sensible heat driven air-pump over the Tibetan Plateau and its impacts on the Asian summer monsoon (in Chinese). *Collection in Memory of Zhao Jiuzhang*, Y. Duzheng, Ed., Chinese Science Press, 116–126.

——, S. Lan, Y. Liu, L. Hui, S. Sun, and W. Li, 2002: Impacts of land surface processes on summer climate. *Selected Papers of the Fourth Conference on East Asia and Western Pacific Meteorology and Climate*, C. P. Chang et al., Eds., World Scientific, 64–76.

——, and Coauthors, 2007: The influence of mechanical and thermal forcing by the Tibetan Plateau on Asian climate. *J. Hydrometeor.*, **8**, 770–789, doi:10.1175/JHM609.1.

——, Y. Guan, T. M. Wang, Y. M. Liu, J. H. Yan, and J. Y. Mao, 2011: Vortex genesis over the Bay of Bengal in spring and its role in the onset of the Asian summer monsoon. *Sci. China Earth Sci.*, **54**, 1–9, doi:10.1007/s11430-010-4125-6.

——, ——, Y. M. Liu, J. H. Yan, and J. Y. Mao, 2012a: Air–sea interaction and formation of the Asian summer monsoon onset vortex over the Bay of Bengal. *Climate Dyn.*, **38**, 261–279, doi:10.1007/s00382-010-0978-9.

——, Y. Liu, B. Dong, X. Liang, A. Duan, Q. Bao, and J. Yu, 2012b: Revisiting Asian Monsoon formation and change associated with Tibetan Plateau forcing: I. Formation. *Climate Dyn.*, **39**, 1169–1181, doi:10.1007/s00382-012-1334-z.

——, Y. M. Liu, B. He, Q. Bao, A. M. Duan, and F. F. Jin, 2012c: Thermal controls on the Asian summer monsoon. *Nat. Sci. Rep.*, **2**, 404, doi:10.1038/srep00404.

Xu, Z. F., C. B. Fu, and Y. F. Qian, 2009: The relative roles of land–sea distribution and orography in the Asian monsoon intensity. *J. Atmos. Sci.*, **66**, 2714–2729, doi:10.1175/2009JAS3053.1.

——, Y. F. Qian, and C. B. Fu, 2010a: The role of land–sea distribution and orography in the Asian monsoon. Part I: Land–sea distribution. *Adv. Atmos. Sci.*, **27**, 403–420, doi:10.1007/s00376-009-9005-7.

——, ——, and ——, 2010b: The role of land–sea distribution and orography in the Asian monsoon. Part II: Orography. *Adv. Atmos. Sci.*, **27**, 528–542, doi:10.1007/s00376-009-9045-z.

Yanai, M., and G.-X. Wu, 2006: Effects of the Tibetan Plateau. *The Asian Monsoon*, B. Wang et al., Eds., Springer, 513–549.

——, S. Esbensen, and J.-H. Chu, 1973: Determination of bulk properties of tropical cloud clusters from large-scale heat and moisture budgets. *J. Atmos. Sci.*, **30**, 611–627, doi:10.1175/1520-0469(1973)030<0611:DOBPOT>2.0.CO;2.

——, C. F. Li, and Z. S. Song, 1992: Seasonal heating of the Tibetan Plateau and its effects on the evolution of the Asian summer monsoon. *J. Meteor. Soc. Japan*, **70**, 319–351.

Ye, D. Z., and Y. X. Gao, 1979: *Meteorology of the Qinghai-Xizang Plateau*. Chinese Science Press, 278 pp.

Yeh, T. C., S.-W. Lo, and P.-C. Chu, 1957: The wind structure and heat balance in the lower troposphere over Tibetan Plateau and its surrounding. *Acta Meteor. Sin.*, **28**, 108–121.

Yu, J. J., Y. M. Liu, and G. X. Wu, 2011a: An analysis of the diabatic heating characteristic of atmosphere over the Tibetan Plateau in winter I: Climatology. *Acta Meteor. Sin.*, **69**, 79–88.

——, ——, and ——, 2011b: An analysis of the diabatic heating characteristic of atmosphere over the Tibetan Plateau in winter II: Interannal variation. *Acta Meteor. Sin.*, **69**, 89–98.

Zhang, J. J., and Coauthors, 1988: *Advances in the Qinghai-Xizang Plateau Meteorology–The Qinghai-Xizang Meteorology Experiment (QXPMEX 1979) and Research.* Chinese Science Press, 268 pp.

Zhang, Y. N., G. X. Wu, Y. M. Liu, and Y. Guan, 2014: The effects of asymmetric potential vorticity forcing on the instability of South Asia high and Indian summer monsoon onset. *Sci. China Earth Sci.*, **57**, 337–350, doi:10.1007/s11430-013-4664-8.

Zhu, X. Y., Y. M. Liu, and G. X. Wu, 2012: An assessment of summer sensible heat flux on the Tibetan Plateau from eight data sets. *Sci. China Earth Sci.*, **55**, 779–786, doi:10.1007/s11430-012-4379-2.